DISSERTATIONES
GEOGRAPHICAE
UNIVERSITATIS
TARTUENSIS
76

IULIIA BURDUN

Improving groundwater table monitoring for Northern Hemisphere peatlands using optical and thermal satellite data

DISSERTATIONES GEOGRAPHICAE UNIVERSITATIS TARTUENSIS
76

DISSERTATIONES GEOGRAPHICAE UNIVERSITATIS TARTUENSIS
76

IULIIA BURDUN

Improving groundwater table monitoring for Northern Hemisphere peatlands using optical and thermal satellite data

UNIVERSITY OF TARTU
Press

Department of Department of Geography, Institute of Ecology and Earth Sciences, Faculty of Science and Technology, University of Tartu, Estonia

Dissertation was accepted for the commencement of the degree of *Doctor philosophiae* in physical geography at the University of Tartu on August 26, 2020 by the Scientific Council of the Institute of Ecology and Earth Sciences University of Tartu.

Supervisors: Dr Valentina Sagris
University of Tartu
Estonia

Prof. Ülo Mander
University of Tartu
Estonia

Opponent: Prof. Margaret Kalacska
McGill University
Canada

Commencement: Senate Hall, University of Tartu, Ülikooli 18, Tartu, on 13 October 2020 at 3.00 p.m.

Publication of this thesis is granted by the Institute of Ecology and Earth Sciences, University of Tartu

ISSN 1406-1295
ISBN 978-9949-03-446-8 (print)
ISBN 978-9949-03-447-5 (pdf)

University of Tartu Press
www.tyk.ee

TABLE OF CONTENTS

LIST OF ORIGINAL PUBLICATIONS

This thesis is based on the following original publications referred to in the text by their Roman numerals:

I. **Burdun I**, Sagris V, Mander Ü (2019) Relationships between field-measured hydrometeorological variables and satellite-based land surface temperature in a hemiboreal raised bog. Int J Appl Earth Obs Geoinf 74:295–301. https://doi.org/10.1016/j.jag.2018.09.019

II. **Burdun I**, Bechtold M, Sagris V, Komisarenko V, De Lannoy G, Mander Ü (2020) A comparison of three trapezoid models using optical and thermal satellite imagery for water table depth monitoring in Estonian bogs. Remote Sens 12:1980. https://doi.org/10.3390/rs12121980

III. Bechtold M, De Lannoy G, Koster RD, Reichle RH, Mahanama S, Bleuten W, Bourgault MA, Brümmer C, **Burdun I**, Desai AR, Devito K, Grünwald T, Grygoruk M, Humphreys ER, Klatt J, Kurbatova J, Lohila A, Munir TM, Nilsson MB, Price JS, Röhl M, Schneider A, Tiemeyer B (2019) PEAT-CLSM: A Specific Treatment of Peatland Hydrology in the NASA Catchment Land Surface Model. J Adv Model Earth Syst 2018MS001574. https://doi.org/10.1029/2018MS001574

IV. **Burdun I**, Bechtold M, Sagris V, Lohila A, Humphreys E, Desai AR, Nilsson M, De Lannoy G, Mander Ü. Satellite determination of peatland water table temporal dynamics by localizing representative pixels of a SWIR-based moisture index. Remote Sens (submitted)

Author's contribution to the articles denotes: '*' a minor contribution, '**' a moderate contribution, '***' a major contribution.

	Articles			
	I	II	III	IV
Original idea	**	***	*	***
Study design	**	***	*	***
Data processing and analysis	***	***	*	***
Interpretation of the results	***	***	*	***
Writing the manuscript	***	***	*	***

LIST OF ABBREVIATIONS

AρρEEARS	Application for Extracting and Exploring Analysis Ready Samples
CLSM	Catchment Land Surface Model
DOY	Day Of Year
FVC	Fractional Vegetation Cover
GEE	Google Earth Engine
GEOS	Goddard Earth Observing System
GHG	Greenhouse Gas
LAI	Leaf Area Index
LST	Land Surface Temperature
MODIS	MODerate-resolution Imaging Spectroradiometer
NDVI	Normalized Difference Vegetation Index
OPTRAM	OPtical TRApezoid Model
PEATCLSM	PEATland-specific adaptation for CLSM
SMAP	Soil Moisture Active Passive
SMOS	Soil Moisture and Ocean Salinity
STR	Shortwave infrared Transformed Reflectance
SWIR	Shortwave Infrared
TOTRAM	Thermal-Optical TRApezoid Model
WT	Water Table
WTD	Water Table Depth
WVPP	Water Vapour Partial Pressure

1. INTRODUCTION

In the last decades, there has been a growing interest in climate change and associated with it carbon cycle (Cox et al. 2000). The particular attention was given to peatlands – a type of wetlands that are defined by at least 30 cm thickness of a surface soil layer storing the partially decomposed vegetation (known as peat). Peatlands cover only 2.84% of the global land area, nevertheless, they store approximately 21% of the global total soil organic C stock (Scharlemann et al. 2014; Xu et al. 2018). Previous studies have demonstrated that there is much more peat C accumulated in northern (75–80%) than in tropical and southern peatlands (10–15%) (Yu 2011; Frolking et al. 2011). Northern peatlands – those located in mid to high latitudes – contain one-third of the global terrestrial carbon that ranges from 250 to more than 1000 Gt (Post et al. 1982; Roulet et al. 2007; Yu et al. 2010). The accumulation of this tremendous amount of carbon took thousands of years and led to the net long-term cooling effect of peatlands on Earth climate (Frolking and Roulet 2007; Yu et al. 2011).

One of the main factors that contribute to carbon accumulation in peatlands is anoxia. Anoxic conditions caused by shallow water table depth (WTD) led to the exceedance of vegetation production over the decays in natural peatlands (Damman 1996). WTD is a position of the water table in the peat layer relative to the ground surface, which alter aerobic to anaerobic conditions in peat and causes a shift in fluxes of greenhouse gases (GHG), particularly CO_2, N_2O and CH_4 (Alm et al. 1999; Salm et al. 2012; Pärn et al. 2018). Deeper WTD exposes peat soil to oxygen, which allows peat aerobic oxidation and leads to increase in CO_2 emissions (Moore and Knowles 1989; Hooijer et al. 2012; Salm et al. 2012). While, shallow WTD inhibit C losses from microbial respiration and leads to anaerobic decomposition and release of CH_4 to the atmosphere (Rosenberry et al. 2003). CH_4 has larger radiative efficiency than CO_2; nevertheless, it has a much shorter lifetime in the atmosphere (Myhre et al. 2013). The study by Günther et al. (2020) suggests that CH_4 emissions from peatlands do not increase the long-term warming effect of the atmosphere, unlike CO_2 emissions, which have negative effects on the magnitude and timing of global warming. Thus, peatlands with shallow WTD act as an ongoing C sink and have a cooling effect on the climate.

Destabilisation of hydrological conditions could turn peatlands from carbon sinks into carbon emission hotspots through the increase of CO_2 emissions (Dorrepaal et al. 2009). The accurate estimation of the hydrological conditions in peatlands is of high interest because it is pivotal for modelling carbon exchange between peatlands and the atmosphere (Limpens et al. 2008). Mitigation of global climate change requires the assessing of greenhouse gases, including those emitted by peatlands. For this, an accurate estimation of WTD in peatlands is needed.

Nowadays, several approaches exist to monitor the WTD dynamics in peatlands. The field-based monitoring is the oldest approach to directly measure WTD in a field. For example, one of the longest field measurements of WTD in

the world is from Männikjärve peatland in Estonia. The monitoring station in this peatland was founded in 1950 and since 1951 the WTD records began (Paal and Leibak 2011; Swindles et al. 2019). Usually, data from one or several monitoring wells are enough to conclude about the general dynamic of WTD in one peatland. Peat soil, in contrast to mineral soils, does not have a watertight layer (Ivanov 1981). This leads to low resistance to horizontal water movement in the upper peat layer within a peatland. Therefore, WTD in peatlands fluctuates rather coherently in space.

However, in some types of peatlands surface runoff can change the local behaviour of WTD. There are two main types of peatlands: bogs, which are only rain-fed, and fens, which are additionally fed with groundwater and, sometimes, surface runoff. Despite bogs and fens are widespread in the northern region (Xu et al. 2018), in-situ data have been collected only in a very limited number of peatlands. The main reasons for that are the high costs and need for much labour for the field campaigns.

Remote sensing, unlike the in-situ data collection, can provide global monitoring of WTD dynamic in peatlands. It relies on physically-based relationships between WTD and peat soil moisture. Usually, strong relationships exist between WTD and peat moisture. This is because of the tight capillary connection between shallow WTD and soil moisture in peatlands (Lindholm and Markkula 1984; Price 1997; Price and Schlotzhauer 1999; Kellner and Halldin 2002; Lafleur et al. 2005b; Kull et al. 2008; Strack and Price 2009). In previous studies, this tight connection was illustrated by scatterplots presenting temporal changes of WTD and soil moisture at an individual location in peatland. In these scatterplots, points of data align in narrow bands, which says that a new soil water equilibrium was quickly established in peat, even after precipitation events. Thus, based on the estimation of peat soil moisture, it is possible to conclude about the position of WTD in peat soil.

Peatlands' soil moisture can be estimated using remotely sensed microwave and optical data. Passive and active microwave sensing enables the estimation of soil moisture due to the large difference between the dielectric constants of water (~80) and dry soil particles (~4) (Entekhabi et al. 2010; Kerr et al. 2010; Ulaby and Long 2014; Dorigo et al. 2017). Because of that microwave remote observations directly reflect the soil moisture in the top few centimetres of the soil. Passive microwave missions, such as Soil Moisture and Ocean Salinity (SMOS) and Soil Moisture Active Passive (SMAP), are equipped with L-band radiometers (Entekhabi et al. 2010; Kerr et al. 2010). The long wavelength of L-band in the passive microwave observations enables accurate estimation of soil moisture by accounting for the vegetation roughness effect. The main disadvantage of passive microwave observations is their coarse resolution (40–50 km), which is inappropriate for monitoring moisture dynamic in peatlands that are usually much smaller in size. However, these observations are used in a global assimilation framework to improve the modelling of WTD in peatlands. For example, SMAP data can be used in the state-of-the-art land surface water and energy budget model Catchment Land Surface Model (CLSM) of the NASA Goddard Earth

Observing System (GEOS) framework (Bechtold et al. 2019a). SMOS L-band brightness temperature was applied to a PEATland-specific adaptation for CLSM (PEATCLSM) (Bechtold et al. 2020).

Active microwave missions, for example, Sentinel-1 (Torres et al. 2012), collecting data of higher spatial resolution. However, an active radar signal is highly affected by land surface properties (Ulaby et al. 1981). In natural peatlands, the confounding effects occur due to scattering in the vegetation and upper fibric peat layer. As a result, active microwave observations have low sensitivity to the WTD in peatlands (Wagner et al. 1999; Bourgeau-Chavez et al. 2007; Bechtold et al. 2018; Zwieback and Berg 2019).

Optical remote sensing with missions such as Landsat, MODerate-resolution Imaging Spectroradiometer (MODIS) and Sentinel-2 allows monitoring of soil moisture indirectly, through the monitoring of spectral properties of the canopy (Jackson et al. 2004; Sadeghi et al. 2017). Optical observations enable the studying of the vegetation conditions, which in turn highly dependent on soil moisture in the rooting zone (Sadeghi et al. 2017). One of the most known methods to estimate soil moisture from optical data is the so-called "trapezoid" or "triangle" model. Two types of trapezoid models exist and they differ in the used moisture-sensitive signal. The first type of the model utilises thermal data – Land Surface Temperature (LST) – and called Thermal-Optical TRApezoid Model (TOTRAM) (Goward et al. 2002; Sandholt et al. 2002; Patel et al. 2009; Mallick et al. 2009; Wang et al. 2011). TOTRAM relies on the physical principle of evaporative cooling (wetter = cooler). The second type of the model – called OPtical TRApezoid Model (OPTRAM) – uses absorption of Shortwave Infrared (SWIR) radiation of water and calculates the Shortwave infrared Transformed Reflectance (STR) from SWIR (Sadeghi et al. 2017). In both types of the model, the moisture-sensitive signal is used together with vegetation index, e.g. the Normalized Difference Vegetation Index (NDVI), the Fractional Vegetation Cover (FVC) or Leaf Area Index (LAI) to construct a trapezoid space (Goward et al. 1985; Carlson et al. 1994; Moran et al. 1994; Carlson 2007; Sadeghi et al. 2017; El Hajj et al. 2017; Carlson and Petropoulos 2019). In this trapezoid space, the lowest LST or highest STR along the vegetation index gradient defines the wettest soil moisture, whereas the highest LST or lowest STR defines the driest soil moisture in the landscape.

Despite trapezoid models, particularly OPTRAM, have high accuracy in estimating soil moisture in mineral soil, yet, their applicability has not been tested for the northern peatlands. In this thesis, I cover this gap of knowledge and discuss the potential of remote sensing techniques, which are based on optical and thermal satellite imagery, for monitoring WTD dynamics in different types of peatlands (i.e. bogs and fens). The novelty of this thesis is that it, for the first time, provides the discussion about the applicability of TOTRAM and OPTRAM in northern peatlands and provides the basis for a future global application of OPTRAM for monitoring WTD in peatlands.

The general aim of the thesis is to improve the monitoring of temporal changes in the position of WTD in the peat layer of northern peatlands with the use of

optical and thermal satellite data. This thesis focuses on specific remote sensing approaches, namely, LST and based on it TOTRAM, and OPTRAM. In this work, I explore the potential of each of this technique to be used for monitoring of WTD. To achieve the general aim, the following tasks were set out:

a) evaluate the applicability of LST data for monitoring hydrometeorological conditions (including WTD) in Estonian peatland (**Article I**);
b) test the performance of two trapezoid models, the first is based on optical and thermal imagery, also known as TOTRAM, and the second one is based on optical imagery alone, also known as OPTRAM for monitoring temporal and spatial dynamic in WTD in two Estonian peatlands (**Article II**);
c) analyse the performance of OPTRAM approach in comparison to modelled PEATCLSM WTD for monitoring temporal dynamic in WTD using long-term (>10 years) dataset for five northern peatlands (**Article III and Article IV**).

2. MATERIALS AND METHODS

2.1. Remotely sensed LST as an indicator of hydrometeorological conditions in one Estonian peatland (Article I)

In **Article I**, we studied the potential of solely taken LST to reflect the hydrometeorological conditions in one peatland, where the long-term in-situ data were available. Here, we explained the variability of LST with in-situ measurements, particularly, we tested the sensitivity of LST to changes in WTD. We conducted this analysis for the growing periods 2008–2016 when LST of peatland vegetation could potentially present vegetation moisture conditions, given the assumption that wetter conditions would be sensed with lower LST.

2.1.1. Study area

We chose Männikjärve peatland in Estonia as a study area because of the long-term (> 60 years) hydrometeorological records available. This peatland located in central Estonia and it has heterogeneous microtopography: hummocks, ridge-hollow and ridge-pool complexes. *Pinus Sylvestris* grows mainly at the peatland's edge (marked as treed bog in Figure 1) and on the ridges. The vegetation of the treeless peatland is presented by *Ledum palustre*, *Vaccinium uliginosum*, *Calluna vulgaris*, *Empetrum nigrum*, and *Sphagnum* species.

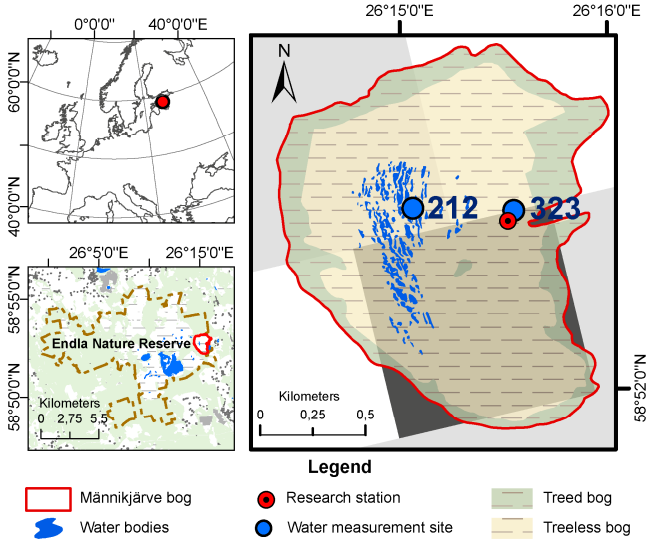

Figure 1. Study area. Water measurement site 212 is located in a pool and data for pool's water table was collected there. Water measurement site 323 is located on organic soil and data of WTD in peat were sampled there. The location of the research station is presented with the red-filled circle; weather data were collected there. The grayscale tetragons represent the MODIS MOD11A1 grid. The darkest grey tetragon represents the MODIS pixel, which time-series data were used in **Article I**. Source: **Article I**, Figure 1.

2.1.2. Research data

In-situ data

To study the sensitivity of LST to hydrometeorological conditions in peatland, we used data for vegetation period of nine years (from May to September 2008–2016). In this research, we used the following in-situ data: TAir – air temperature (measured at a height of 2 m every 3 h), Prec – precipitation (measured once a day), WVPP – water vapour partial pressure (measured every 3 h), TSoil – soil temperature at depths of 5, 10, 15, 20 cm and TSurf – surface temperature (measured every 6 h), WT 212 – water table in peatland pool and WTD 323 – WTD in peat soil (Figure 1).

Remotely sensed data

We used LST time-series data sensed by MODIS Terra mission obtained through AρρEEARS (Application for Extracting and Exploring Analysis Ready Samples https://lpdaacsvc.cr.usgs.gov/appeears/). LST data from MODIS were chosen because of the high temporal resolution of these data – MODIS overpasses the study area every day and provides with the daily-based measurements. However, MODIS LST suffers from the coarse spatial resolution – 1 km. Our study area was covered by several MODIS pixels, but only one of them was more than 90% covered with peatland. In further analyses, the time-series of LST for this pixel was used (Figure 1).

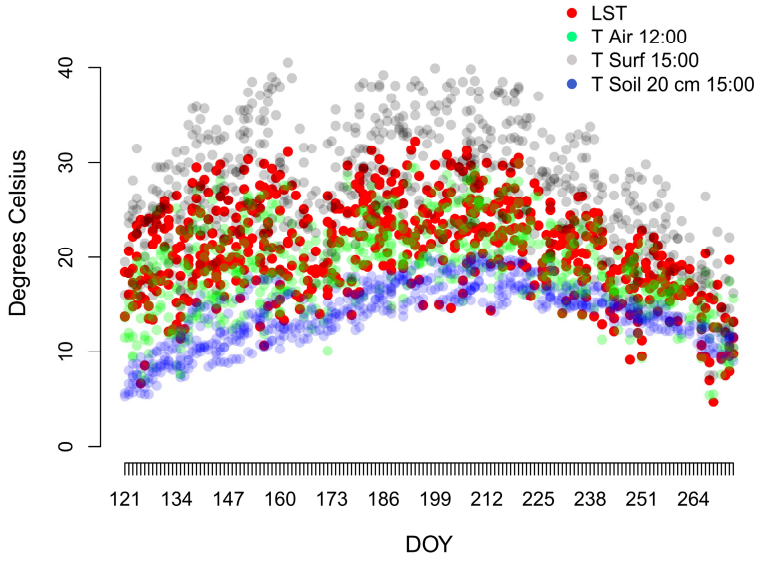

Figure 2. Variability of field-measured temperature with LST from the beginning of May till the end of September 2008–2016 (121–274 days of the year). TAir at 12:00, TSurf and TSoil at 15:00 are presented only for the days when LST was sensed. Source: **Article I**, Figure 3.

The footprint of the selected pixel mainly corresponds to the peatland area; however, some areas of forest at mineral soil are also present within this pixel. For the pre-test, we plotted time-series data of LST and in-situ TAir, TSurf and TSoil to determine whether pixel's LST signal corresponds to the thermal conditions in the peatland (Figure 2). Generally, the seasonal curve of LST matches a lot with those for TAir, TSurf and TSoil. It is seen that TSurf at 15:00 was, usually, higher than LST while TAir at 12:00 was much similar to LST values. Based on this, we concluded that the LST values of the selected MODIS pixel reflect the thermal condition of the peatland. Thus, despite this pixel includes some small area of forest, its LST values are still representative of the studied peatland.

2.1.3. Statistical analysis

With the reason to account for a cumulative effect of temperature and precipitation, we summarised TAir, TSurf, TSoil and Prec for last 5 and 10 days before LST was sensed. Further, the summarised time-series was used together with the raw time series.

The linear association between the hydrometeorological observations and LST was examined using Pearson correlation analysis (R) in R software (R Core Team 2018). We calculated R between data for a) each year, b) each month over the different years, c) total period of study.

A multiple linear regression was used to model relationships between the in-situ predictors and remotely sensed LST for each month (from May to September) over the different years. A linear regression method was applied to standardized variables. The mean-centre method was chosen to standardise the data. Regression diagnostics were done to the hydrometeorological data. A random forest approach together with forward selection was used to fit the regression models.

2.2. Estimation of TOTRAM and OPTRAM for monitoring changes in WTD in two Estonian peatlands (Article II)

After assessing the potential of LST solely to reflect hydrometeorological conditions, we aimed to test the applicability of two trapezoid models to monitor changes in WTD in peatlands. The first trapezoid model – TOTRAM – utilises LST together with vegetation index, the second model – OPTRAM – utilises STR instead of LST, and vegetation index. In **Article II,** we extended the study period (growing seasons in 2008–2019) and study area (two peatlands), and we used remotely sensed data of higher spatial resolution (30 m). Here, we estimated TOTRAM and OPTRAM based on Landsat 5, 7 and 8 data. Landsat spatial

resolution of tens of metres integrates soil moisture small-scale variability over hummock and hollow microtopography (Figure 3), but in comparison to MODIS resolution, it is still informative to analyse the spatial patterns of moisture indices.

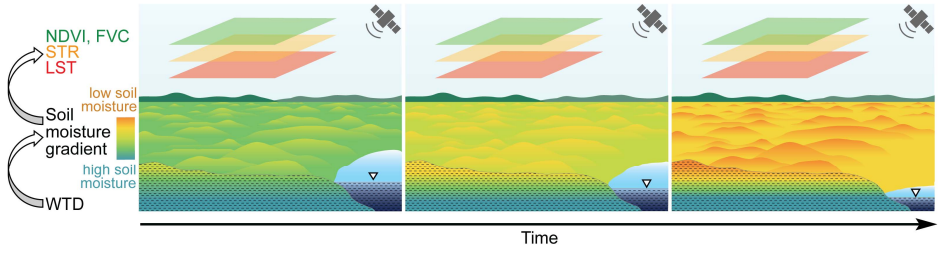

Figure 3. Sketch illustrating the concept of the link between WTD and remotely sensed parameters via the capillary connection between WTD, moisture in the soil, and vegetation. The remotely sensed parameters used in this study: NDVI, FVC, LST and STR. Source: **Article II**, Figure 1.

Given the assumption that WTD and surface soil moisture have a tight capillary connection, we hypothesise that remotely sensed moisture indices, i.e., TOTRAM and OPTRAM, are sensitive to the changes in WTD in peatlands (Figure 3). In this article, we evaluated the temporal and spatial correlation of the TOTRAM and OPTRAM based on in-situ measured WTD.

2.2.1. Study area

In **Article II** we extended the study area to two Estonian peatlands: Linnusaare and Männikjärve (Figure 4). The in-situ data from Männikjärve peatland were previously used in **Article I**. Both peatlands are of limnogenic origin and located within the East-Baltic Bog Province (Sillasoo et al. 2007). The tree layer of both bogs consists mainly of sparse *Pinus sylvestris*. The grass and dwarf shrub layers consist of *Calluna vulgaris*, *Eriophorum vaginatum*, *Chamaedaphne calyculata* (Burnett et al. 2003). The typical moss species are *Sphagnum fuscum, Sphagnum balticum, Sphagnum magellanicum,* and *Sphagnum rubellum* (Burnett et al. 2003).

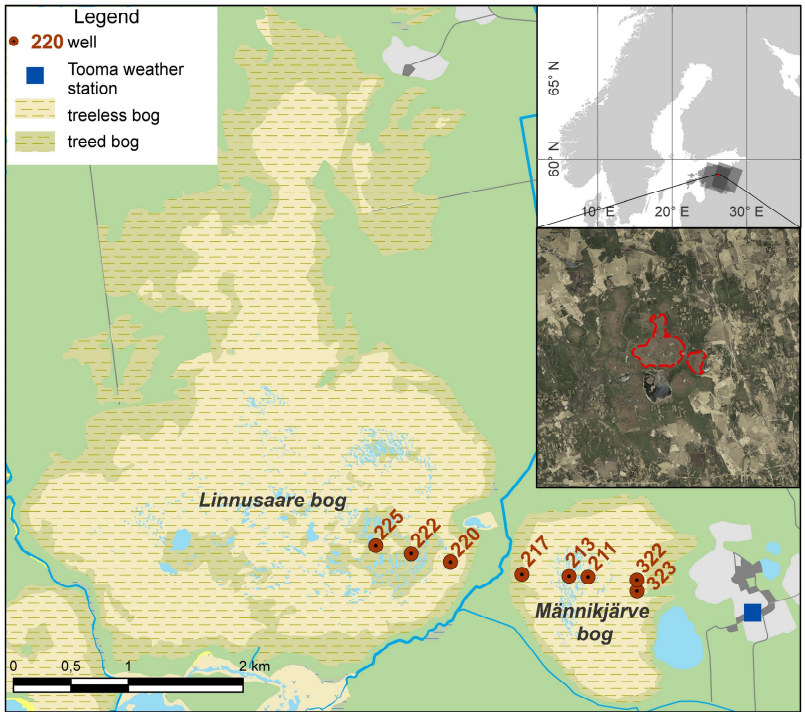

Figure 4. Base map showing the study area of **Article II**: Linnusaare and Männikjärve bogs with (red circles) locations of water table measurement sites, (blue square) weather station, and (green shading) treed and treeless bog areas (designed by authors based on data from Estonian Topographic Database, Land Board 2020 (Estonian Land Board 2020)). The upper inset presents (dark grey) two overlapping Landsat scenes and (red square) the clipped area used in the modelling of trapezoids. The lower inset is a zoom of the clipped area and highlights the two bogs (red polygons). Source: **Article II**, Figure 3.

2.2.2. Theoretical concepts of trapezoid models

TOTRAM: Thermal-Optical Trapezoid Model

TOTRAM is one of the most widely used remote sensing approaches to estimate surface moisture in mineral soils (Goward et al. 2002; Sandholt et al. 2002; Mallick et al. 2009; Zhang et al. 2015; Capodici et al. 2020). This approach is based on the trapezoidal-shaped distribution of pixel values in the space defined by LST and a vegetation index, for example, FVC, NDVI or LAI (Nemani et al. 1993; Carlson et al. 1994; Moran et al. 1994) (Figure 4). The highest and lowest values of LST along the vegetation cover gradient represent the so-called dry and wet edges (Figure 4). In addition to the wet and dry edges, more isopleths can be drawn indicating transitional moisture conditions (Prihodko and Goward 1997). The moisture condition of each pixel, W_{TOTRAM}, is estimated based on its location relative to the dry and wet edges within the trapezoidal-shaped distribution of pixels in a single scene,

$$W_{TOTRAM,i} = \frac{LST_{max,i} - LST_i}{LST_{max,i} - LST_{min,i}} \quad (1)$$

where LST_i is the LST value of the pixel i and $LST_{max,i}$ and $LST_{min,i}$ are the LST values of the dry and wet edge at FVC_i (Figure 5a).

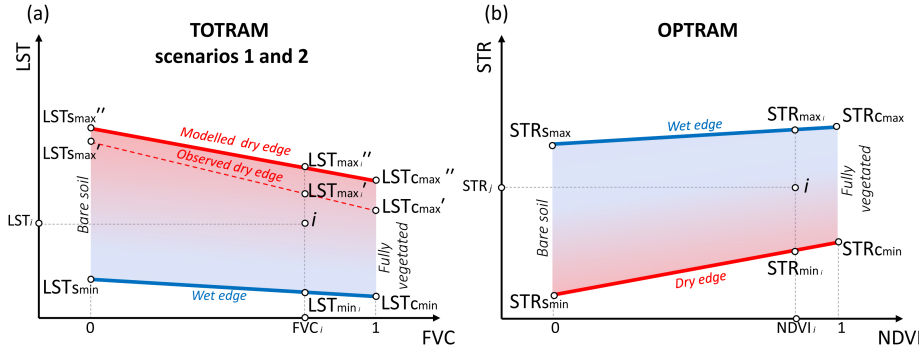

Figure 5. Illustration of the concept of: (**a**) TOTRAM; and (**b**) OPTRAM. For TOTRAM, both the observed (Scenario 1) and the modelled (Scenario 2) dry edges are presented. The dry edges are indicated by points $LSTs_{max}'$ and $LSTc_{max}'$ for TOTRAM Scenario 1, $LSTs_{max}''$ and $LSTc_{max}''$ for TOTRAM Scenario 2, and $STRs_{min}$ and $STRc_{min}$ for OPTRAM. The wet edges are indicated by points $LSTs_{min}$ and $LSTc_{min}$ for both TOTRAM scenarios, and $STRs_{max}$ and $STRc_{max}$ for OPTRAM. The colour gradient shows the soil moisture availability from blue (wet edge) to red (dry edge). Point i is a surface with LST_i, FVC_i, STR_i, and $NDVI_i$. For i within LST-FVC space, the temperature of the wet edge is $LST_{min,i}$, observed dry edge is $LST_{max,i}'$, and modelled dry edge is $LST_{max,i}''$. For i within STR–NDVI space, the STR value for the wet and dry edge are $STR_{max,i}$ and $STR_{min,i}$, respectively. Source: **Article II**, Figure 2.

TOTRAM approach has several limitations. It requires, firstly, that the location of the isopleths within LST-VI space is determined by the water availability and not by the difference in atmospheric conditions. For this reason, TOTRAM is not applicable to mountain regions and to the images sensed on different days. Secondly, LST decreases not only in space but also in time with increasing values of vegetation index (Price 1990; Gillies et al. 1995). In this study, we applied two TOTRAM scenarios from literature, they mainly differ in the treatment of these application criteria in the context of the dry edge determination.

Scenario 1: Observed dry edge

In TOTRAM Scenario 1, the dry and wet edges were determined from the observed highest and lowest LST values along the FVC gradient following the algorithm in (Tang et al. 2010). Following this algorithm, we split the LST pixels based on FVC values in LST–FVC space into 20 intervals and each interval into 5 subintervals. For each interval, the minimum and maximum LST values were calculated. After, the wet and dry edges were modelled as the linear fit to the mentioned minimum and maximum LST values.

Scenario 2: Modelled dry edge

For the accurate determination of wet and dry edges TOTRAM approach requires sufficient variability of land surface moisture (Carlson 2007). However, after widespread precipitation events, the dry edge can not be defined because of the lack of pixels representing the dry areas. To overcome this limitation, it has been proposed to derive the dry edge theoretically, i.e. based on models (Zhang et al. 2008; Long and Singh 2012; Zhang et al. 2014). The modelled dry edge was determined by two modelled temperatures: the temperature of the driest bare surface ($LSTs_{max}''$) and the driest fully vegetated surface ($LSTc_{max}''$) (Figure 5a). We followed the algorithm for retrieving $LSTs_{max}''$ and $LSTc_{max}''$ developed by Long et al. (2012), which is based on solving for the system of physically-based non-linear equations in an iterative manner (**Article II** Appendices A and B). We applied Scenario 2 for a shorter period (2009–2019) than Scenario 1 (2008–2019) because the in-situ meteorological measurements needed for modelling the dry edge were only available starting from June 2009.

OPTRAM: Optical Trapezoid Model

OPTRAM approach was introduced by Sadeghi et al. (Sadeghi et al. 2017) as an alternative to TOTRAM. OPTRAM utilises STR instead of LST as a soil moisture-sensitive parameter (Figure 5b). In OPTRAM, the trapezoid is formed by NDVI as a measure of vegetation cover and STR as a measure of moisture content (Sadeghi et al. 2015). In contrast to TOTRAM approach, OPTRAM allows merging the data sensed on different days for constricting one joint trapezoid space. To determine the wet and dry edges, firstly, we randomly sampled 10% of the pixels from the total dataset. Secondly, the full range of sampled NDVI values was divided into 100 intervals. Within each interval, the median, standard deviation, maximum, and minimum STR values were obtained. The dry edge was modelled as a linear fit to the minimum STR values. The dry edge was modelled as a linear fit to the "median + standard deviation" values of the 100 intervals. To exclude the pixels that correspond to water bodies, we filtered out pixels with negative NDVI before the OPTRAM calculation.

The OPTRAM soil moisture index, W_{OPTRAM}, is then derived using the equation:

$$W_{OPTRAM,i} = \frac{STR_i - STR_{min,i}}{STR_{max,i} - STR_{min,i}} \quad (2)$$

where STR_i is the STR value of the pixel i, while the $STR_{max,i}$ and $STR_{min,i}$ are the STR values of the dry and wet edge at the NDVI of pixel i (Figure 5b).

2.2.3. Research data

In-situ data

We used air temperature and air pressure measured at an hourly resolution at Tooma weather station, which is located on the mineral soil close to the study area (Figure 4). The data were available beginning from June 2009. Additionally, we used WTD data from eight monitoring wells installed in hollows along a transect (Figure 4). Daily measured WTD data for the growing seasons (May–September) 2008–2019 were used in this study.

Reanalysis and remotely sensed data

ERA 5 is the atmospheric reanalysis of the global climate produced by the European Centre for Medium-Range Weather Forecasts (Hersbach et al. 2020). We used ERA 5 data of friction velocity and total column water vapour for modelling of the dry edge required for TOTRAM Scenario 2 (**Article II** Appendices A and B).

For LST estimation we utilised brightness temperature data of Landsat 5, 7 and 8, emissivity data of MODIS and water vapour data of NCEP/NCAR datasets. NDVI, FVI and surface albedo were calculated based on data of Landsat 5, 7 and 8.

Variable Derivation

The basic workflow of data preparation is presented in Figure 6. This figure shows the analysis steps with data inputs and outputs. Data processing was performed on the Google Earth Engine (GEE) online platform (Gorelick et al. 2017). The final TOTRAM and OPTRAM calculation and statistical analyses were performed in R software (R Core Team 2018). The detailed description of the data preparation steps can be found in **Article II**.

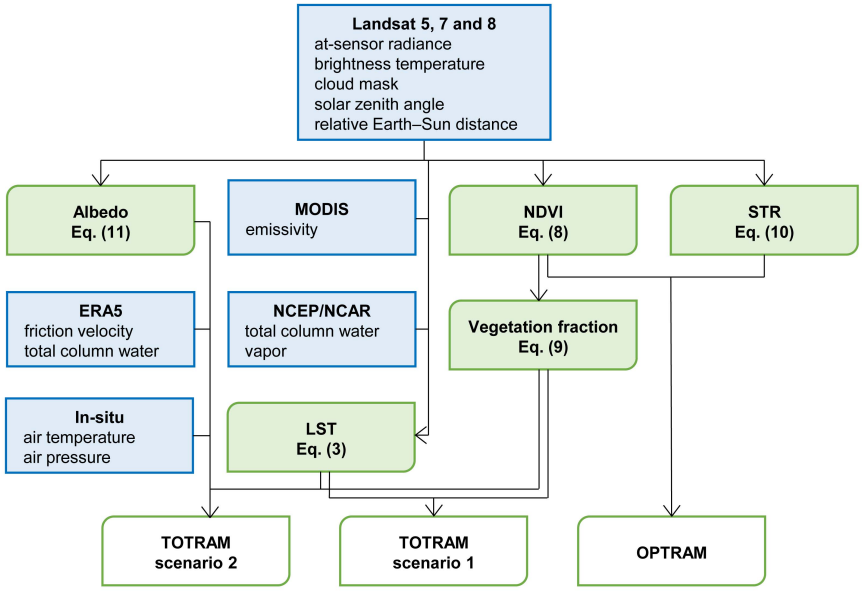

Figure 6. Data preparation for the two TOTRAM scenarios and OPTRAM. Blue-filled rectangles represent input parameters and variables and green-filled rectangles with diagonal corners rounded represent intermediate parameters and variables. The numbers of equations refer to the equations presented in **Article II**. Source: **Article II**, Figure 4.

2.2.4. Statistical analysis

We calculated the temporal Pearson correlation coefficients (R) between soil moisture indices of the three different trapezoid models (TOTRAM scenarios 1 and 2, and OPTRAM) and in situ WTD measurements. Anomaly Pearson correlation coefficients (anomR) were calculated to evaluate the capability of the trapezoid models to monitor the variability of WTD. Anomaly time series of in-situ and soil moisture indices were obtained by removing the multi-year one-month-smoothed average from the original time series values.

2.3. Testing OPTRAM performance in five northern peatlands by comparison with PEATCLSM WTD (Article III and IV)

In **Article III**, we assessed the accuracy of up-to-date modelling techniques for estimation of the modelled WTD. Later, in **Article IV** we compared the performance of OPTRAM index in comparison to the modelled WTD. **Article IV** addresses the challenges of OPTRAM application that we faced with and described in **Article II**, particularly: dependency of OPTRAM representativeness for WTD monitoring from vegetation cover, and a limited number of peatlands where OPTRAM was tested. Since the sensitivity of OPTRAM index to changes in WTD depends highly on vegetation cover, in this work we suggest an approach, which can localize OPTRAM pixels with the highest sensitivity to WTD (further called 'best pixels').

In **Article IV** we suggest that 'best pixels' can be localised using in-situ WTD (if such is available) or WTD modelled by a land surface model (if no in-situ records are available) (Figure 7). Given the assumption that WTD varies rather coherently within a peatland, in-situ measurements from one monitoring well are sufficient to determine the overall temporal variation of WTD in a peatland. The localizing of the 'best pixels' on the basis of WTD measured in-situ allows estimating the temporal changes in WTD beyond the time period for which in-situ records are available. However, the in-situ WTD is measured only in a small number of peatlands. To provide the basis for a future global application of OPTRAM over northern peatlands, we propose localizing the 'best pixels' by the use of WTD data modelled by a land surface model with PEATCLSM (Ducharne et al. 2000; Koster et al. 2000; Bechtold et al. 2019a).

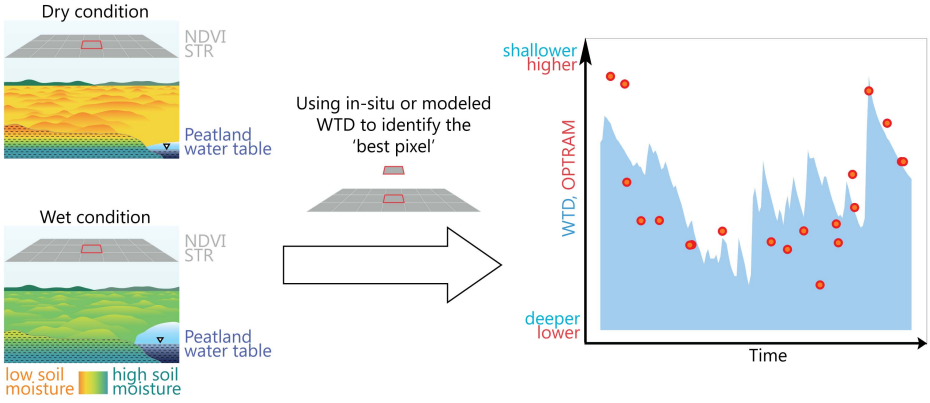

Figure 7. Schematic illustration of the approach proposed in this study. The 'best pixel' for the monitoring of water table depth (WTD) with OPTRAM index can be localized by measured or modelled WTD data when assuming that WTD varies uniformly within a peatland. Source: **Article IV**, Figure 1.

Article IV seeks to address the challenges of OPTRAM application in peatlands to localize the 'best' OPTRAM pixels for monitoring WTD by using either in-situ or modelled WTD data. In this study, we used data of five northern peatlands (fens and bogs) where long-term records of in-situ WTD were available. We, firstly, compared the performance of OPTRAM based on different spatial resolutions (namely, Landsat, MODIS and Landsat spatially rescaled to the MODIS resolution); secondly, compared the performance of applying in-situ and PEATCLSM WTD data for selecting the 'best' OPTRAM pixels; thirdly, assessed the quality of OPTRAM index in comparison to PEATCLSM WTD data for WTD monitoring.

Besides, we seek to compare the performance of 'best' OPTRAM pixels with modelled PEATCLSM WTD for the need of in-situ WTD monitoring. The PEATCLSM WTD data were obtained as model output in **Article III**.

2.3.1. PEATCLSM simulation and modelled WTD data (Article III)

In **Article III** we addressed the problem of poor representation of peatlands in global Earth system models nowadays. Here, we suggest using the new module for monitoring hydrological conditions in peatlands, namely, PEATCLSM. This suggested module accounts for peat hydraulic properties and performed better in comparison to basic CLSM simulation.

The basic structure of CLSM was used in combination with peatland-specific parameters taken from the literature sources. We compared the performance of PEATCLSM (ExpC) with one simulation that used CLSM with default mineral soils (ExpA), and the second simulation that used CLSM with the updated peat soil parameters (ExpB) in northern peatlands. A more detailed description of simulations is given in Section 2 of **Article III**.

For this research, the unprecedentedly large data set of WTD was used: data from 94 monitoring wells and 44 peatlands (22 bogs and 22 fens). All the peatlands are located in the Northern Hemisphere between 40°N and 75°N (Appendix A in **Article III**). We compared the performance of tree simulations using these data of in-situ WTD.

Comparing to ExpA and ExpB scenarios, overall, PEATCLSM outputs significantly better agree with in-situ WTD (Figure 8): the R values are 0.64 for bogs and 0.66 for fens, average bias is –0.12 m, the average root-mean-squared difference is 0.19 m, and average unbiased root-mean-squared difference is 0.10 m. For the unfrozen period between January 1988 through December 2017, PEATCLSM resulted in mean WTD of –0.20 m with a standard deviation of 0.10 m.

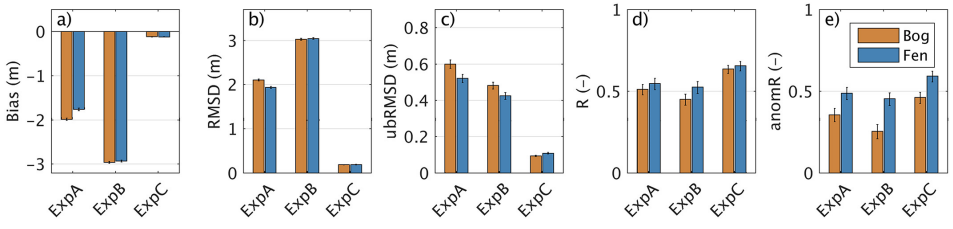

Figure 8. Groundwater table depth (a) bias (model-minus-observation), (b) root-mean-squared difference (RMSD), (c) unbiased root-mean-squared difference (ubRMSD), (d) time series correlation coefficient (R), and (e) anomaly time series correlation coefficient (anomR) for the 30″ simulations (ExpA, ExpB, and ExpC), computed separately for bogs and fens. Bog metrics are based on 55 sites collected into 14 regional clusters. Fen metrics are based on 39 sites collected into 11 regional clusters. The anomR metric is computed from slightly fewer sites (44 and 38, respectively, with 11 clusters each). The time period (1988–2017) varies per site depending on data availability and the length of snow and freezing periods, which were excluded. Also shown are 95% confidence intervals. Source: **Article III**, Figure 6.

Further, in **Article IV** we used PEATCLSM WTD data at 30'' spatial and 3-hourly temporal resolutions presented in Bechtold et al. (2019b). PEATCLSM simulation output contains data from 1988 to 2017 years. PEATCLSM data were used for the same days when in-situ WTD and remotely sensed data were available. We extracted one grid cell PEATCLSM output for each peatland at the times nearest to the Landsat acquisition times.

2.3.2. Study area and in-situ WTD data

In **Article IV**, we used data of five peatlands that is a subset of WTD data from **Article III.** We selected only those peatlands, that have more than 10 years of in-situ WTD data to ensure that the study sites were covered by a sufficient number of remote sensing images (Figure 9). The studied peatlands included two bogs and three fens (Table 1). Table 1 presents a short overview of the peatlands studied in **Article IV**. All of these peatlands have at least 30 cm thickness of the peat layer and shallow WTD.

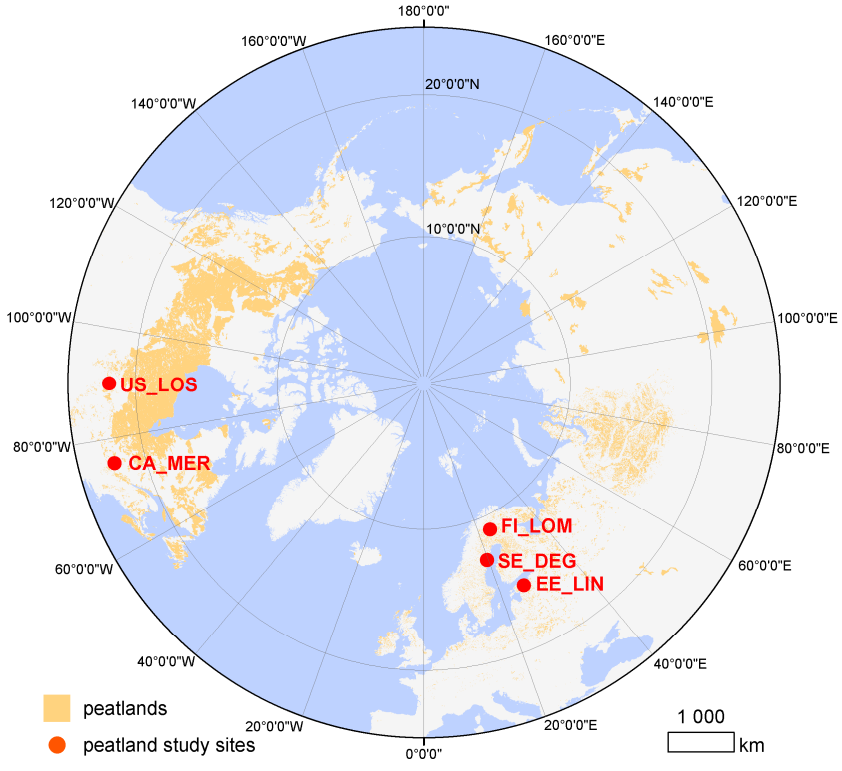

Figure 9. Study sites (red dots) used in **Article IV** and distribution of northern peatlands (based on Xu et al. (2018)). Source: **Article IV**, Figure 2.

Table 1. Overview of peatland sites

Site name and location	Site code	WTD data period	Peatland type	Dominant vegetation	Lat.	Lon.	Ref.
Linnusaare, Estonia	EE_LIN	2008–2017	bog	Mosses, sedges, shrubs, sparse dwarf pines	58.88	26.20	**Article I**
Mer Bleue, Canada	CA_MER	2000–2017	bog	Shrubs, sedges, black spruce, mosses	45.41	–75.52	(Lafleur et al. 2005a; Strilesky and Humphreys 2012)
Degerö Stormyr, Sweden	SE_DEG	2002–2017	fen	Sedges, mosses, shrubs	64.18	19.55	(Peichl et al. 2013)
Lompolojänkkä, Finland	FI_LOM	2006–2017	fen	Sedges, low shrubs, mosses, downy willows and dwarf birch	67.99	24.20	(Aurela et al. 2009; Aurela et al. 2015)
Lost Creek, USA	US_LOS	2000–2017	fen	Alder, willow, sedges	46.08	–89.97	(Sulman et al. 2009)

2.3.3. OPTRAM estimation and parameterisation

We estimated OPTRAM index using Landsat, MODIS and Landsat rescaled to the MODIS resolution for the period covering in-situ WTD measurements. We conducted our research over the vegetation period (from May to October) to exclude periods when the peat soil was frozen. Data processing was performed on the Google Earth Engine (GEE) online platform (Gorelick et al. 2017). All the remotely sensed data were re-projected to WGS 84 / Pseudo-Mercator projection (EPSG:3857).

Landsat SWIR data of band 7 (2.08–2.35 μm in Landsat 5 and 7, and 2.107–2.294 μm in Landsat 8) was used for STR calculation. The respective spectral difference of the Landsat SWIR band is a source of the potential bias for STR calculation, which was beyond the scope of our methodological framework. To compare the performance of OPTRAM of various spatial resolution, we also estimated OPTRAM based on data from the MODIS aboard Terra MOD09GA with 500 m spatial resolution. The surface reflectance for MODIS band 7 (2.105–2.155 μm) was used for the STR calculation. Landsat and MODIS SWIR data have different ranges of bands used for the STR calculation. To eliminate the effect of different spectral resolutions, we upscaled the 30-m Landsat data (further called Landsat_30m) to the 500-m MODIS resolution (Landsat_500m), in this way, allowing an assessment of the OPTRAM for various spatial resolutions, while using the same spectral information. The new values of Landsat_500m pixels were estimated as the mean value of the Landsat_30m pixels using the function "reduceResolution()" in GEE. It should be noted that the calculation of mean has the inherent bias of dependency on the extreme values. A comparison of upscaling approaches was, however, beyond the scope of our study.

In **Article IV**, in contrast to **Article II**, we estimated dry and wet edges of OPTRAM trapezoid space subjectively, based on the visual inspection of NDVI – STR scatterplots. This approach is common and widely used with OPTRAM (Sadeghi et al. 2017; Babaeian et al. 2018; Mananze and Pôças 2019; Huang et al. 2019; Chen et al. 2020; Ambrosone et al. 2020). We chose this approach for **Article IV** because for some peatlands we observed inadequate determination of wet edges with the approach used in **Article II**. Therefore, we here determined the wet and dry edges subjectively using the visual inspection of NDVI – STR scatterplots for each peatland separately.

2.3.4. Statistical analysis

Prior to estimating temporal correlation coefficients, we tested the normality of variables' distributions with the Kolmogorov-Smirnov test (p-value 0.05). A normal distribution was observed for all the variables except in-situ WTD at CA_MER and US_LOS peatlands (p-values were 0.001 and 0.03 respectively). During the pre-test, we calculated both Pearson and Spearman correlation coefficients for those sites and results were consistent. Thus, for simplicity, we

only provide Pearson correlation coefficients for all sites, including CA_MER and US_LOS.

For each comparison of OPTRAM indices with WTD, the per-pixel temporal Pearson correlation coefficients (R) and anomaly Pearson correlation coefficients (anomR) were estimated. This was done for OPTRAM indices obtained with Landsat_30m, MODIS, and Landsat_500m, and for WTD either in-situ or modeled with PEATCLSM. Anomalies were obtained by removing the multi-year one-month smoothed average from the original values.

We performed a random sampling test to validate the stability of spatial patterns of temporal per-pixel correlation. Two randomly selected subsets, each containing 50% of total data in each peatland, were used to calculate R between OPTRAM and in-situ WTD (Article IV, Figure S2).

For each of the three versions of OPTRAM as well as PEATCLSM WTD, 95% confidence intervals (CIs) of the 'best pixels' correlation coefficients were estimated, first, for each site, taking into account the reduction of the sample size due to temporal autocorrelation (as in (De Lannoy and Reichle 2016; Bechtold et al. 2019a)). We then aggregated the CIs of the five sites, again separately for each of the three versions of OPTRAM as well as PEATCLSM WTD, by dividing the average of the CIs by the square root of the number of sites (De Lannoy and Reichle 2016; Bechtold et al. 2019a). Only one 'best pixel' was localized as the one with the highest statistically significant (p-value < 0.05) R values calculated between OPTRAM index and WTD (either in-situ or modelled) in each peatland.

3. RESULTS

3.1. Dependency of LST on hydrometeorological parameters in Estonian peatland (Article I)

3.1.1. Relationships between LST and hydrometeorological parameters

Figure 10 shows the correlation matrix with the monthly and total R values. Generally, LST had the highest R values with TAir, TSurf and TSoil. The strongest R was observed between LST and TAir 12:00: monthly R values varied between 0.78–0.89, R value for the total period of time was 0.87. In Figure 10, it is seen that relationships between LST and WTD 323 were not statistically significant in May and September; however, in other months and for the whole period of study we observe the weak negative R values between LST and WTD 323.

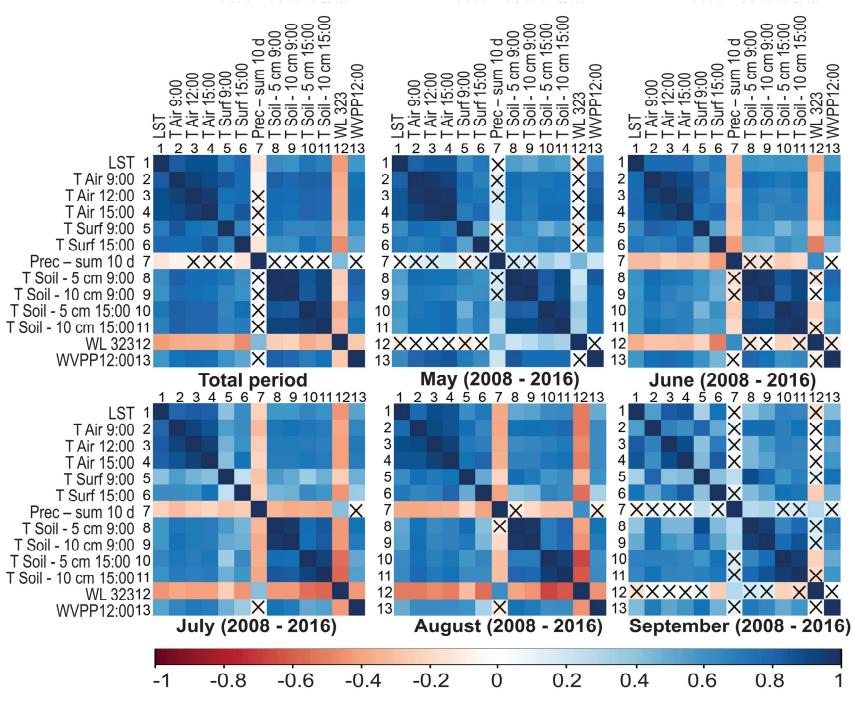

Figure 10. A correlation matrix with R values. TAir – air temperature at 9:00, 12:00 and 15:00, TSurf – surface temperature at 9:00 and 15:00, Prec – sum 10 d – cumulated precipitation of the last 10 days, Tsoi – soil temperatures at the depths of 5 and 10 cm at 9:00 and 15:00, WL 323 (WTD 323 in the text) – water table depth at the measurement point № 323, and WVPP 12:00 – water vapour partial pressure at 12:00 in the total study period and the individual months. The crossed-out cells have a p-value >0.05, the rest have a p-value <0.05. Source: **Article I**, Figure 5.

3.1.2. Main hydrometeorological drivers of LST

Table 2 presents the results of multiple linear regression analysis between hydrometeorological drivers and LST for each month (from May to September) over the 2008–2016 years. The adjusted R^2 is presented in the order in which variables were added to the models. It can be seen, that TAir was the main factor of monthly changes of LST. WTD and WT were significant predictors of LST and included in the linear models with a negative association with LST in May, June and July.

Table 2. Results of the multiple linear regression.

	Estimated	**Std. error**	**t value**	**Pr(>|t|)**	**Adj. R^2**
			May		
Intercept	0.15	0.05	3.01	0.003	
T_{Air} 12:00	0.65	0.06	11.09	<0.001	0.721
WT 212	–0.21	0.07	–2.92	0.004	0.747
T_{Surf} 15:00	0.22	0.07	3.18	0.002	0.765
Prec – sum 10 d	–0.18	0.07	–2.48	0.015	0.776
Residual std. error: 0.41 on 107 degrees of freedom, Multiple R^2.: 0.78, Adjusted R^2.: 0.78, F-statistic: 97.14 on 4 and 107 DF, p-value: < 0.001					
			June		
Intercept	0.04	0.06	0.64	0.524	
T_{Air} 15:00	0.54	0.13	4.23	<0.001	0.632
T_{Air} 9:00	0.37	0.14	2.66	0.009	0.651
WTD 323	–0.10	0.05	–2.09	0.038	0.661
Residual std. error: 0.54 on 116 degrees of freedom, Multiple R^2.: 0.67, Adjusted R^2.: 0.66 , F-statistic: 78.42 on 3 and 116 DF, p-value: < 0.001					
			July		
Intercept	0.12	0.08	1.55		
T_{Air} 15:00	0.52	0.093	5.53	<0.001	0.671
T_{Air} 9:00	0.41	0.09	4.14	<0.001	0.701
WTD 323	–0.15	0.043	–3.41	<0.001	0.709
$T_{soil\text{-}5\ cm}$ 9:00 – sum 10 d	–0.24	0.08	–3.06	0.003	0.726
Residual std. error: 0.3985 on 131 degrees of freedom; Multiple R^2.: 0.73, Adjusted R^2.: 0.73; F-statistic: 90.46 on 4 and 131 DF, p-value: <0.001					

Table 2. Continue

	Estimated	Std. error	t value	Pr(>|t|)	Adj. R^2
August					
Intercept	–0.09	0.034	–2.81	0.006	
T_{Air} 12:00	0.758	0.06	13.27	<0.001	0.784
T_{Surf} 15:00	0.194	0.05	3.59	<0.001	0.804
Residual std. error: 0.35 on 115 degrees of freedom; Multiple R^2.: 0.81, Adjusted R^2.: 0.80; F-statistic: 241 on 2 and 115 DF, p-value: <0.001					
September					
Intercept	–0.20	0.06	–3.17	0.002	
T_{Air} 15:00	0.72	0.06	11.49	<0.001	0.735
T_{Air} 12:00 – sum 10 d	0.45	0.11	4.24	<0.001	0.761
$T_{soil\text{-}5\ cm}$ 9:00 – sum 10 d	–0.27	0.11	–2.41	0.018	0.772
Residual std. error: 0.38 on 103 degrees of freedom; Multiple R^2.: 0.78, Adjusted R^2.: 0.77; F-statistic: 120.5 on 3 and 103 DF, p-value: <0.001					

3.2. Performance of TOTRAM and OPTRAM for estimation changes in WTD in two Estonian peatlands (Article II)

3.2.1. Temporal Correlation of Soil Moisture Indices with WTD

Figure 11 presents boxplots (for eight wells) of the temporal correlation coefficients between in-situ WTD and three moisture indexes (two TOTRAM scenarios and OPTRAM) as average values across four pixels closest to the wells. TOTRAM Scenarios 1 and 2 resulted in negative average R (–0.19 and –0.16, respectively) and anomR (–0.23 and –0.08, respectively) values. OPTRAM resulted in positive R and anomR with average values of 0.41 and 0.37, respectively.

Figure 12 illustrates exemplarily time series for four of twelve years of WTD and TOTRAM Scenarios 1 and 2, and OPTRAM. Time series are presented for monitoring wells 323 (treeless bog, Figure 12a) and 225 (treed bog, Figure 12b) as an average value across four pixels closest to the wells. Time series in Figure 12 shows that soil moisture indices estimated from TOTRAM Scenarios 1 and 2 do not agree with temporal changes in WTD. In contrast, the OPTRAM soil moisture index follows reasonably well the WTD dynamics, in particular in the treeless bog. However, some obvious outliers are still present in OPTRAM time-series.

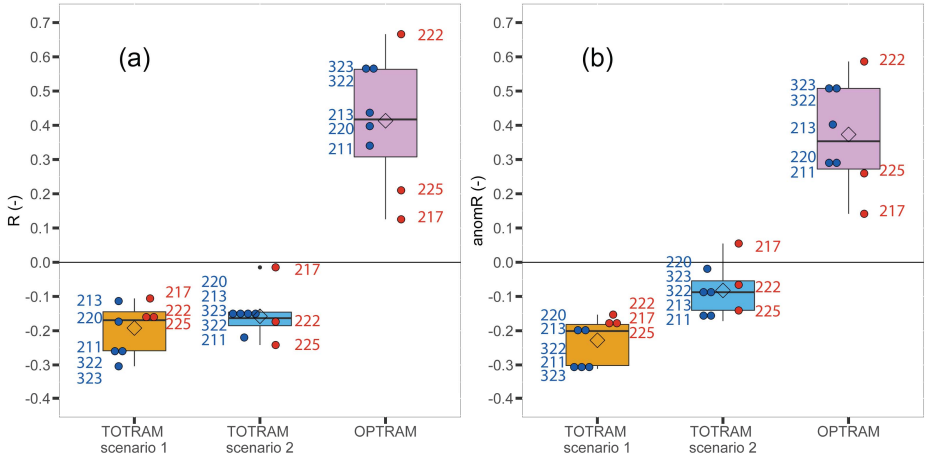

Figure 11. Temporal Pearson correlation coefficient for (**a**) original (R) and (**b**) anomaly time series (anomR) for TOTRAM Scenario 1, TOTRAM Scenario 2, and OPTRAM. Dots present the value of R and anomR of individual wells (numbers as indicated in Figure 4) in treed (red) and treeless (blue) parts of the bog. Boxplots present the distribution of all wells with the bold line indicating the median value and the diamond representing the mean value. Source: **Article II**, Figure 6.

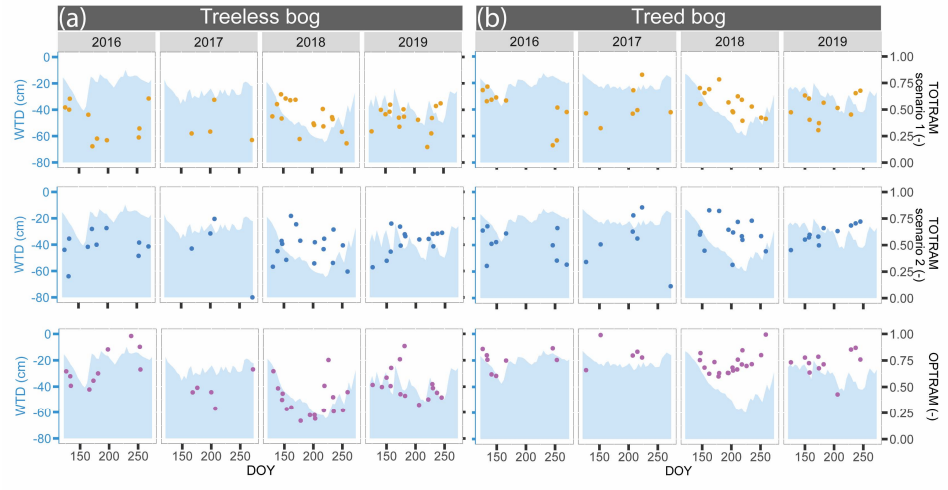

Figure 12. Time series of water table depth (WTD) and soil moisture index from TOTRAM Scenario 1, TOTRAM Scenario 2, and OPTRAM. Time series are exemplarily shown for four years of data from monitoring wells 323 (**a**) in a treeless part and 225 (**b**) in a treed part of the bogs. Source: **Article II**, Figure 7.

Given the assumption that WTD fluctuates coherently in peatlands, we calculated the mean WTD of the eight monitoring wells. Further, we estimated the temporal per-pixel R between mean WTD and three different soil moisture indices. Thus,

the resulting spatial differences in R were assumed to be dominated by the local specifics of the temporal relationship between the WTD and soil moisture index. Figure 13 shows that both TOTRAM scenarios resulted in R values close to zero. However, R values for OPTRAM are positive throughout the whole peatlands area. The highest OPTRAM R values (0.7–0.8) can be observed for treeless areas.

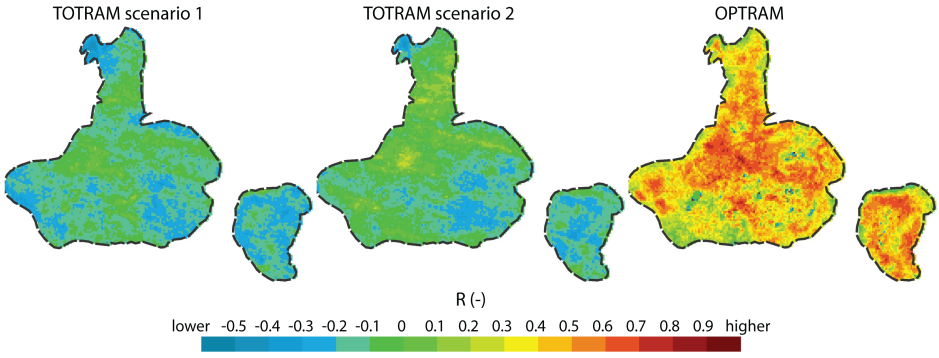

Figure 13. The long-term per-pixel temporal correlation coefficient (R) estimated for the mean water table depth from all eight monitoring wells and soil moisture indices derived from TOTRAM Scenario 1, TOTRAM Scenario 2, and OPTRAM. Source: **Article II**, Figure 8.

3.2.2. Spatial Variability of Soil Moisture Indices and WTD

Figure 14 shows scatterplots, regression line and R values between the moisture indices and WTD across all times for two exemplary monitoring wells (same as in Figure 12). It is seen that only the OPTRAM index shows a positive correlation over the entire WTD range (Figure 12c). Moreover, it is shown that OPTRAM values are systematically higher over treed parts of the bogs and lower over treeless parts of the bogs.

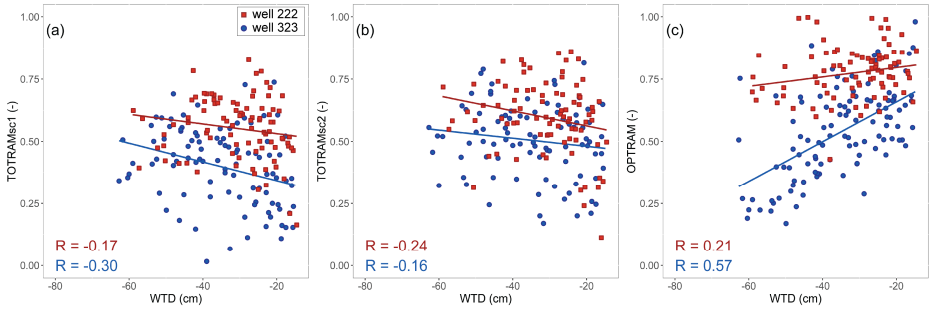

Figure 14. Soil moisture index from (**a**) TOTRAM Scenario 1, (**b**) TOTRAM Scenario 2, and (**c**) OPTRAM as a function of water table depth (WTD) measured in wells 225 (treed) and 323 (treeless). TOTRAMs and OPTRAM values are presented as an average of four pixels the closest to the wells. Source: **Article II**, Figure 9.

Figure 15 shows spatial patterns of TOTRAM Scenario 1, TOTRAM Scenario 2 and OPTRAM for an exemplary wet (5 May 2016) and dry (23 August 2018) conditions. None of the trapezoid models could show plausible variability in soil moisture. For 23/08/2018 it was expected to observe drier soil moisture and deeper WTD towards the margins. However, the opposite can be observed for OPTRAM, while TOTRAM Scenarios 1 and 2 show little variability. On 05/05/2016 the deepest WTD was at wells 217 and 222, which are installed in the treed parts of the peatlands. The OPTRAM index, however, did show relatively high values around those two wells.

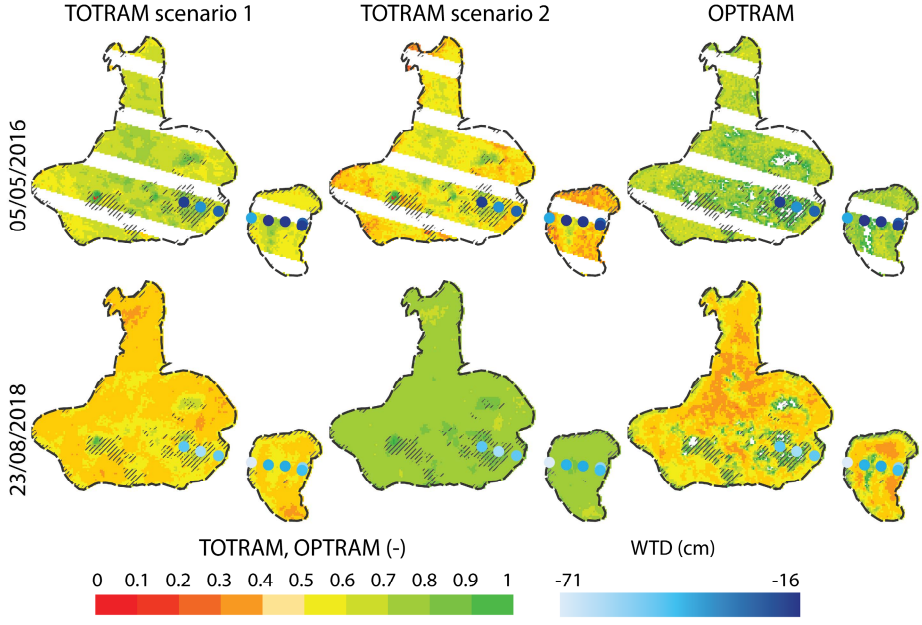

Figure 15. Maps of soil moisture index generated with TOTRAM Scenario 1, TOTRAM Scenario 2, and OPTRAM together with indicated water table depth (WTD) for each monitoring well. The white areas within the bogs represent missing data resulting from Landsat 7 Scan Line Corrector failure (striped pattern on 05/05/2016) or methodological constraints (filtering of oversaturated pixels in OPTRAM). The black hatched pattern indicates the treed bog areas. Source: **Article II**, Figure 10.

Figure 16 presents the maps of the anomaly time series of TOTRAM scenarios and OPTRAM, for four exemplary dates and the corresponding soil moisture anomaly averaged over eight monitoring wells. There is again a good agreement between anomalies in WTD and OPTRAM index. In contrast, the TOTRAM scenarios did not yield changes that could be related to WTD.

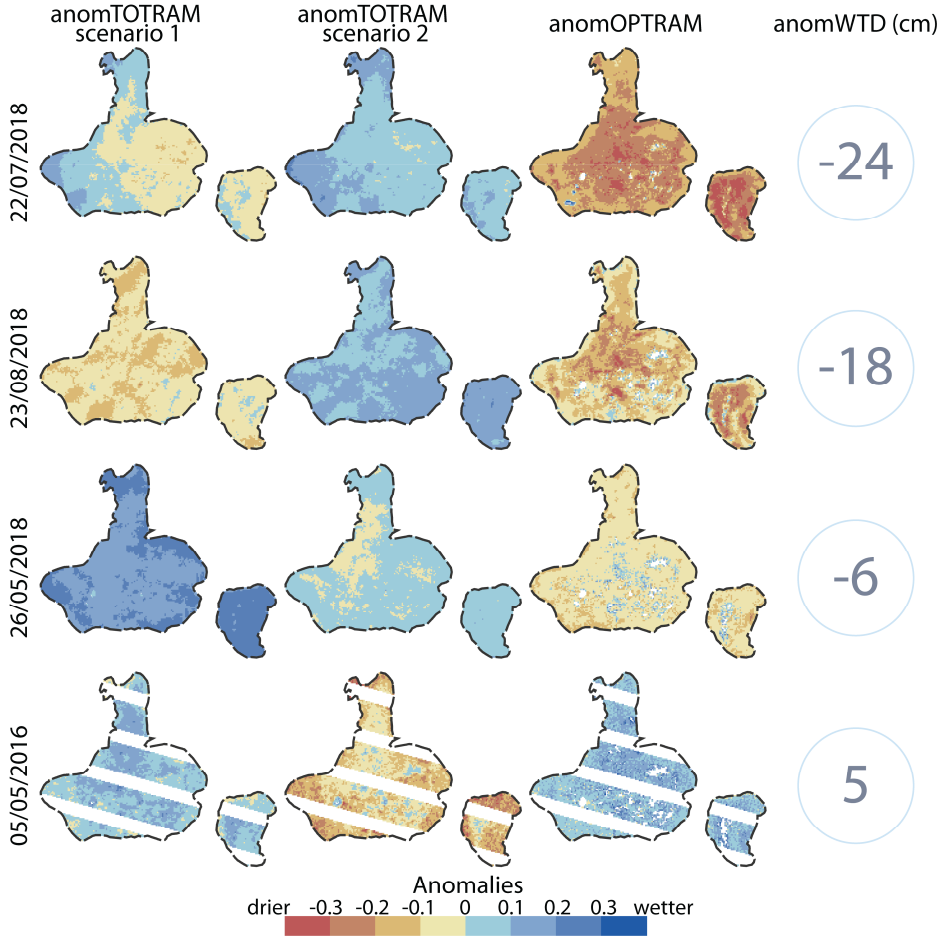

Figure 16. Maps of anomalies in soil moisture index derived from TOTRAM Scenario 1, TOTRAM Scenario 2, and OPTRAM for four exemplary dates and corresponding anomalies in water table depth (anomWTD) averaged over all the monitoring wells. The white areas within the bogs represent missing data resulting from Landsat 7 Scan Line Corrector failure (striped pattern on 05/05/2016) or methodological constraints (filtering of oversaturated pixels in OPTRAM). Source: **Article II**, Figure 11.

3.3. Usefulness of the 'best' OPTRAM pixels to study WTD dynamic in comparison to modelled PEATCLSM WTD (Article III and IV)

3.3.1. Spatial patterns of temporal correlation between OPTRAM and WTD

In **Article IV,** our first task was to evaluate the applicability of OPTRAM based on remotely sensed data of various spatial resolutions for monitoring temporal changes in WTD measured in-situ in northern peatlands. Figure 17 presents the maps of per-pixel R values between in-situ WTD and OPTRAM based on MODIS (panels a–e), Landsat_30m (panels f–j) and Landsat_500m (panels k–o) data for five studied peatlands. It is noticeable, that the strength of R varied depending on the remote sensing data used for the OPTRAM estimation.

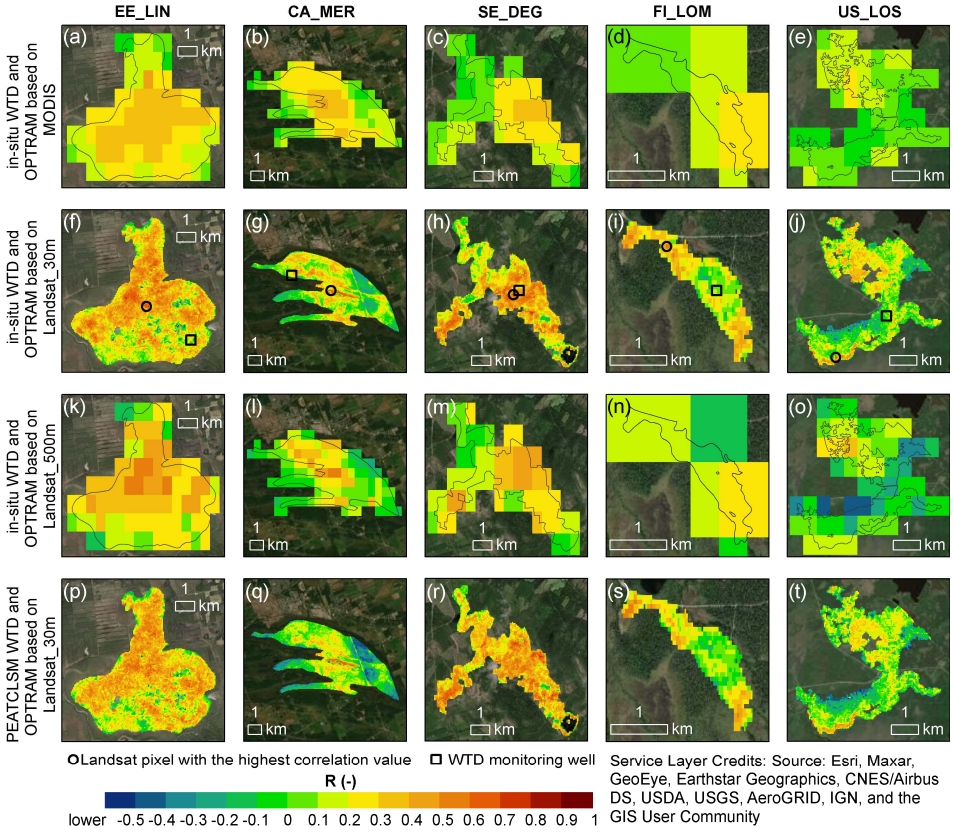

Figure 17. The temporal per-pixel correlation (R) between in-situ water table depth (WTD) and OPTRAM based on Landsat_30m (a–e), MODIS (f–j) and Landsat_500m (k–o), and between WTD modelled with PEATCLSM and OPTRAM based on Landsat_30m (p-t). Panels f–j show the location of the monitoring wells (black square) and the pixels of Landsat_30m data with the highest temporal correlation with in-situ WTD, i.e. the 'best pixel' (black circle). Source: **Article IV**, Figure 5.

Despite MODIS and Landsat_500m have the identical spatial resolution, Landsat_500m yielded higher values of maximum R metrics. The highest values of maximum correlation with in-situ WTD were observed for OPTRAM based on Landsat_30m.

I need to highlight here, that for all peatlands except for SE_DEG, the highest R values between in-situ WTD and OPTRAM based on Landsat_30m were not located close to the WTD monitoring wells (Figure 16, panels f–j). This result supports our initial assumption that in-situ WTD fluctuates rather uniformly within a peatland in time. Thus, it suggests searching in a wider radius for a 'best' OPTRAM pixel.

3.3.2. Dependency of the temporal correlation between OPTRAM and WTD on vegetation cover

Furthermore, we were interested in types of vegetation cover that led to high (> 0.5) and low (< 0.1) R values between in-situ WTD and OPTRAM based on Landsat_30m. For this reason, we analysed available maps of vegetation in the studied peatlands and summarized the results in Table 3. Mainly, areas dominantly covered with mosses and graminoids with very shallow WTD (hollows or lawns) or permanently flooded conditions showed the highest sensitivity of OPTRAM to changes in WTD. The lowest sensitivities of OPTRAM to changes in WTD were present in the areas dominantly covered with shrubs and trees.

Table 3. Overview of vegetation cover attributed to the high and low correlation between WTD and OPTRAM

Site code	Characteristics of sites with high R	Characteristics of sites with low R
EE_LIN	Hollow-ridge complex with permanently flooded depressions. Pixels' area is mainly covered with hollows (Estonian Land Board 2019; Estonian Land Board 2020). The dominant vegetation is *Sphagnum* species and graminoids (Lode et al. 2017).	Hummocks covered with dwarf pines, graminoids and *Sphagnum* species (Keskkonnaagentuur 2002).
CA_MER	A higher density of hollows microtopography with lower plant area index (Arroyo-Mora et al. 2018). Vegetation is dominated by *Sphagnum* species, evergreen shrubs, deciduous shrubs, and sedges (Sonnentag et al. 2007; Li et al. 2007; Kalacska et al. 2013).	Relatively dense tree canopy of black spruce and tamarack (Strilesky and Humphreys 2012; Arroyo-Mora et al. 2018); drained areas east of ditch with gray birch, tamarack and white pine (Talbot et al. 2010).

Table 3. Continue

Site code	Characteristics of sites with high R	Characteristics of sites with low R
SE_DEG	Permanently flooded *Sphagnum*-dominated hollows, lawns and flarks (Arens 2017; Osterwalder et al. 2018; Nijp et al. 2019).	Forested peatland with pine and spruce (ICOS 2018).
FI_LOM*	A high percentage of *Sphagnum* cover (70–98%). Sites are covered with mosses, graminoids, shrubs and trees. This territory matches with the area covered by vegetation community described as cluster 3 (Räsänen et al. 2019).	Corresponds to riparian areas of the stream running through the FI_LOM site. It is primarily vegetated by 60-cm-high Salix (Räsänen et al. 2019).
US_LOS	Emergent or wet meadows, and lowland shrubs (2019).	Forested wetland and shrubs (2019).

* vegetation data available only for the central part of the peatland

3.3.3. Temporal relationships between in-situ WTD and OPTRAM, and between in-situ and modelled WTD

Another objective was to reveal how well the OPTRAM index is agreed with in-situ WTD in comparison to PEATLCSM simulations obtained in **Article III**. Figure 18 shows 'best pixel' with the highest R value (Figure 17) together with its anomR value for each peatland. In addition, Figure 17 presents R and anomR values between in-situ WTD and PEATCLSM WTD. It is seen, that the highest mean R between in-situ WTD and OPTRAM was obtained OPTRAM based on Landsat_30m. Moreover, the high temporal R and anomR values between in-situ WTD and OPTRAM based on Landsat_30m are almost as good as those between in-situ WTD and WTD modelled with PEATCLSM. Nonetheless, both the OPTRAM based on Landsat_30m and PEATCLSM WTD performed worse in FI_LOM site because peat soil was inundated most of the time. For PEATCLSM data the R and anomR were estimated for the same days as for Landsat_30m. The correlation metrices for the whole period of time when in-situ WTD data were available can be found in **Article III** Table A2. Generally, values R and anomR between in-situ and modelled WTD are very alike in **Article III** and **Article IV**.

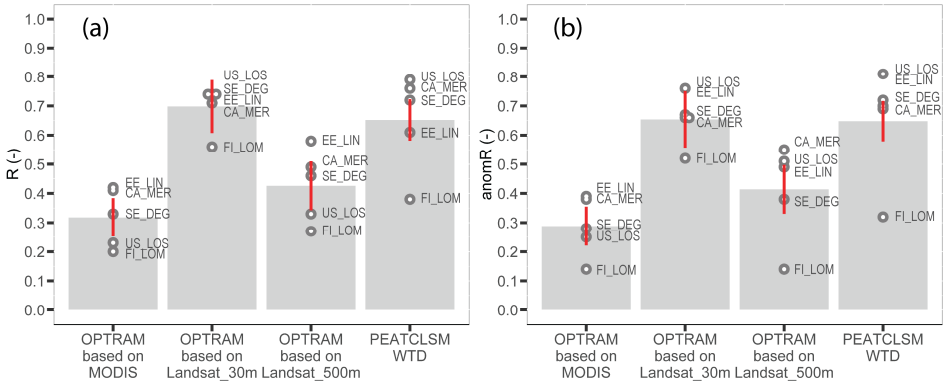

Figure 18. Temporal Pearson correlation coefficients between in-situ water table depth (WTD) and 3 versions of OPTRAM as well as PEATCLSM WTD for (a) original (R) and (b) anomaly (anomR) time series data. R and anomR are shown only for pixels with the highest R value within each peatland site, i.e. the 'best pixel', and for PEATCLSM WTD and in-situ WTD (data taken for the same days as for estimating R between in-situ WTD and OPTRAM based on Landsat_30m). The black dots and text on the right-hand side of these dots present the R and anomR values of the selected pixel and site code where this pixel is located. The height of the bars indicates the mean value of R and anomR. The error bars represent the 95% confidence intervals after having taken into account the temporal autocorrelation. Source: **Article IV**, Figure 6.

To show the relationships between in-situ WTD and OPTRAM Landsat_30m which are presented with the correlation values in Figure 18, Figure 19 presents scatterplots of those two variables together with scatterplots of in-situ WTD vs PEATCLSM WTD. On average, OPTRAM based on Landsat_30m and PEATCLSM performed very similar: R values ranged from 0.56 to 0.74 (average 0.7) for OPTRAM based on Landsat_30m, and from 0.38 to 0.79 (average 0.65) for PEATCLSM WTD.

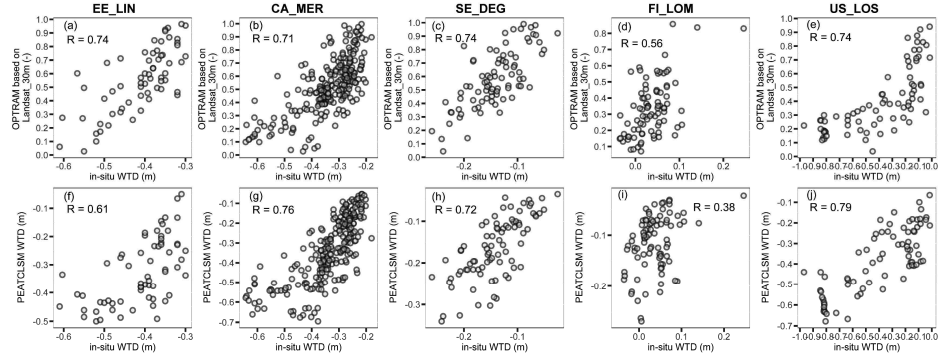

Figure 19. Scatterplots of (panels a–e) in-situ water table depth (WTD) and OPTRAM based on Landsat_30m 'best pixel', and (panels f–j) in-situ WTD and PEATCLSM WTD taken for the same days as for OPTRAM based on Landsat_30m and in-situ WTD. Source: **Article IV**, Figure 7.

The time series of in-situ WTD, OPTRAM based on Landsat_30m and PEATCLSM WTD for three consecutive years are given in Figure 20.

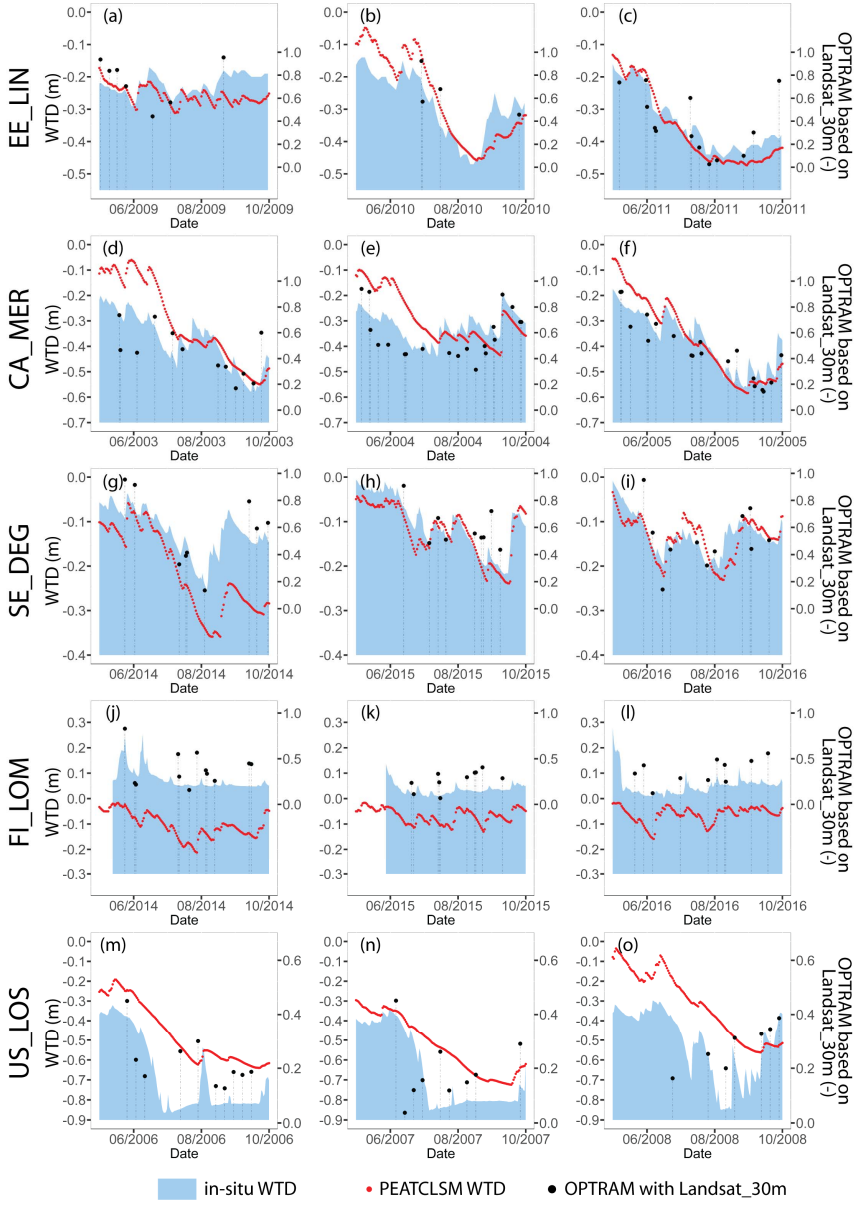

Figure 20. Exemplary three-year periods of the long-term time series of water table depth (WTD) measured in situ and modelled with PEATCLSM, and OPTRAM based on Landsat_30m. OPTRAM values are shown for the 'best pixel' within each peatland site. For better visual comparison, the OPTRAM range is adjusted to the in-situ WTD range of each site for the shown period. Source: **Article IV**, Figure 8.

To illustrate the consistency in time dynamics between those variables, the OPTRAM range was adjusted to the in-situ WTD range of each site for the shown period. It can be seen, that OPTRAM values exhibit the seasonal cycle of in-situ WTD (especially in SE_DEG and CA_MER sites) and short-term dynamics of in-situ WTD for all peatlands, except for FI_LOM, where the lowest agreement between OPTRAM and in-situ WTD is observed.

4. DISCUSSION

4.1. The weak correlation between LST and TOTRAM index with in-situ WTD in Estonian peatlands

All the satellite imagery, used in the thesis, have the inherent error bias related to mission-specific geometric distortions. Such distortions originate from a wide range of factors, such as the following: sensor optics view angle, scanning system motion and orientation, satellite stability and velocity, land relief and its dynamics, Earth curvature and rotation. These factors likely influenced the raw satellite imagery, but since we relied on the post-processed products distributed by AρρEEARS and GEE, their accounting was beyond the scope of our study.

The results from the **Article I** suggest that solely taken LST is a strong predictor of thermal conditions within the peatland; however, it is a weak predictor of in-situ WTD. We found out that in June, July and August LST had a negative statistically significant R with WTD. It could be, firstly, because of the cooling effect of the shallower WTD in peat layer (Weiss et al., 2006); secondly, because of the increase of vegetation productivity during the summer months (Harris 2008; Letendre et al. 2008; Péli et al. 2015).

In **Article I,** we faced several limitations of LST data: the coarse spatial resolution of MODIS data and associated with that only one pixel used in the analyses. To overcome those limitations and to explore deeper the potential of LST for WTD monitoring, we used Landsat data of higher spatial resolution in **Article II**. We estimated LST-based TOTRAM moisture index, which in theory should correlate positively with in-situ WTD. Although TOTRAM has been used as a good indicator of soil moisture in other studies (Garcia et al. 2014; Holzman et al. 2014; Sadeghi et al. 2017), we did not observe the strong positive association with WTD in peatland for both scenarios of TOTRAM. Here we provide two main aspects of TOTRAM that hampered its applicability to our study area; both aspects are related to the generally wetter conditions in northern latitude ecosystems.

The first limitation is that the TOTRAM indices were computed per each day of observation. This limits the ability to constrain the trapezoid space with both dry and wet surfaces present. We attempted to overcome this limitation with modelling the dry edge for TOTRAM Scenario 2; however, this did not improve the performance of TOTRAM approach.

The second reason for the lack of correlation between WTD and TOTRAM indices might be that vegetation growth is much more limited by energy than by moisture in the northern region (McVicar et al. 2012). Karnieli et al. (2010) described that in high latitude regions, warming is accompanied by vegetation growth and, thus, LST and VI have a positive association.

These results suggest a general inapplicability of the LST and LST-based TOTRAM index for the temporal WTD monitoring in northern peatlands. Nevertheless, LST can be used as a strong predictor of thermal conditions.

4.2. Factors affecting the ability of OPTRAM to reveal the changes in WTD

This thesis showed that the ability of OPTRAM to detect the changes in WTD depends mainly on two factors: (i) the spatial resolution used for OPTRAM estimation, and (ii) vegetation cover within OPTRAM pixel.

Results of **Article II** and **Article IV** demonstrates a high potential of the OPTRAM index with a high spatial resolution (Landsat_30m) to monitor temporal changes of WTD dynamics in different types of peatlands. This is the point to which the current thesis contributes. The good temporal correlation statistics suggest that OPTRAM of high spatial resolution might be a new type of observation used for global monitoring of WTD in peatlands. The worse performance of lower spatial resolution (Landsat_500m or MODIS) could be explained by the high fragmentation of vegetation cover, which is in hummock – hollow/ lawn complexes in peatlands. 500-m sized pixel seems to be insufficient to capture the SWIR signal comes from vegetation communities, which have the highest OPTRAM sensitivity to changes in WTD (Figure 21).

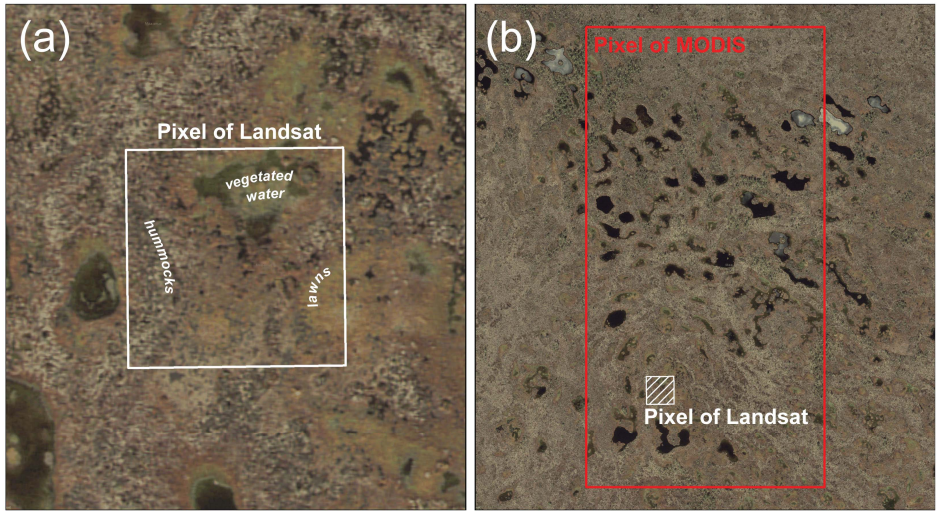

Figure 21. Comparison of the area represented by one Landsat pixel (a) and one MODIS pixel (b). The location of the Landsat_30m 'best pixel' in EE_LIN site is shown. Source: **Article IV**, Figure 9.

The performance of OPTRAM varied for data with a similar spatial resolution, i.e. Landsat_500m and MODIS. A first possible explanation for this might be the difference in their SWIR bands used for the STR calculation. Landsat data with longer SWIR wavelengths resulted in a higher maximum temporal R values with in-situ WTD than the MODIS data with shorter SWIR wavelengths. This result agrees with the previous study, which illustrates the better performance of longer SWIR wave for mineral soil moisture estimation (Sadeghi et al. 2015). This is a

promising finding, which shows a high potential for Sentinel-2 data (SWIR 2.10–2.28 μm) to be used for OPTRAM estimation to monitor WTD changes in peatlands. Previous studies indicated that data of narrow SWIR band (wavelengths 2.3 μm) from hyperspectral imagery are highly sensitive to the vegetation conditions in different ecosystems, including wetlands (Serbin et al. 2015; DuBois et al. 2018). Future studies may be focused on the applicability of OPTRAM based on hyperspectral imagery to reveal the WTD dynamic in peatlands.

A second possible explanation for the different performance of OPTRAM based on MODIS and Landsat_500m could be the different temporal frequency of remotely sensed data. The difference in MODIS and Landsat temporal resolutions leads to a larger number of MODIS observations than Landsat_500m ones. Therefore, these results need to be interpreted with caution.

4.3. OPTRAM performance in different types of peatlands: bogs and fens

In our study, we observed that OPTRAM performance was similar in bogs and fens; both types of peatlands resulted in similar high temporal correlation metrics. Only in FI_LOM site we observed a weak correlation between in-situ WTD and OPTRAM. It might be because FI_LOM was the only site in our database with very high and stable in-situ WTD, and thus, the vegetation growing on permanently saturated peat soil might have a less explicit response to changes in soil moisture and WTD. Harris et al. (2005) described a similar effect on Sphagnum mosses, which have an uneven curve of the relationship between remotely based moisture stress index (utilises SWIR and near-infrared spectra) and volumetric moisture content in the peat soil. Interesting to notice, that for other studied sites, where WTD fluctuates much more in time, areas with shallow WTD and without tree cover performed the highest correlation metrics between OPTRAM and in-situ WTD. In contrast, the areas of weak sensitivity of OPTRAM to WTD dynamic were covered with trees and shrubs in both types of the peatlands.

4.4. Potential of using in-situ and PEATCLSM WTD for selecting the OPTRAM pixels with the highest sensitivity to WTD fluctuations

In **Article II** we revealed the issue that OPTRAM sensitivity to changes in WTD highly varies between vegetation cover. We found that pixels of treeless peatland yielded much higher temporal correlation with in-situ WTD than pixels of treed peatland. Thus, we highlighted the need for localizing OPTRAM pixels, which are the most sensitive to temporal changes in in-situ WTD, i.e. 'best pixels'. In **Article IV** we suggested applying in-situ and modelled WTD data for selecting the 'best pixels'. For this purpose, we used modelled PEATCLSM WTD generated in **Article III**.

The results presented in Figure 17 suggest that both in-situ and modelled WTD can be used to localize the 'best' OPTRAM pixels. The patterns of R values in panels f–j of Figure 16 are highly consistent with those shown in panels p–t; and in both cases, they are attributed to certain vegetation cover within the peatlands. This finding supports the hypothesis that both in-situ and modelled WTD can be used interchangeably to detect the 'best' OPTRAM pixels. A concrete application would be to find the 'best' OPTRAM pixel based on historical simulations or in situ data and subsequently use OPTRAM data at this pixel to monitor WTD near real-time.

Although our results indicated a high potential of localizing 'best pixels' for OPTRAM by using PEATCLSM WTD, there is the risk of selection bias towards zones in a peatland area that are conform to model physics used in PEATCLSM. The coherence of the WTD fluctuations in peatland is not perfect, and, e.g., variable input fluxes of minerotrophic water, which are not simulated in PEATCLSM, generate some spatial variation of WTD dynamics. Similarly, a selection of the 'best pixel' based on only a single in situ location will always be biased towards the WTD dynamics of that specific location. These two limitations are important to keep in mind when using monitoring data based on the 'best pixel' approach.

4.5. Quality assessment of OPTRAM in comparison to PEATCLSM

We showed in **Article IV** that OPTRAM based on Landsat_30m and PEATCLSM WTD yielded similar correlation metrics with in-situ WTD (Figure 18). For EE_LIN, FI_LOM and SE_DEG sites OPTRAM performed slightly better than PEATCLSM WTD. This better performance of OPTRAM can be explained by the fact that PEATCLSM can not reflect all the fluctuations in in-situ WTD either due to the coarse resolution global forcing data (was shown in **Article III**) or lack of local peatland processes such as the variable dependency of fens to minerotrophic water inputs.

Based on the good temporal correlation statistics together with a feasible application for long-term monitoring, we suggest that OPTRAM index could be suitable for assimilation into the peatland-specific hydrological models. OPTRAM index has the potential to contribute independent information to PEATCLSM by providing valuable peat moisture information at high spatial resolution. Moreover, long-term Landsat observations (started from 1972) have great potential to be used for revealing decade-long WTD changes in peatlands driven by climate change and also anthropogenic disturbances that are not accounted for in PEATCLSM.

The future challenge is to determine the reason for the OPTRAM outliers detected in **Article II** and **Article IV**. The identification of the reasons for these outliers and methods to filter them out will be critical for future global OPTRAM application for monitoring WTD dynamics in peatlands.

5. CONCLUSIONS

This thesis evaluated the relationships between in-situ measured WTD and remotely sensed indicators of moisture conditions, namely, LST and tree different trapezoid models, two of them are based on thermal and optical data (TOTRAM), and one – optical data solely (OPTRAM). We conducted this study to reveal the potential of mentioned techniques to be used for monitoring changes in WTD in northern peatlands. Based on the results obtained in each article, the following conclusions are formulated:

- LST solely is a moderate predictor (R = 0.35–0.5) of WTD in Estonian peatland. Our study demonstrated that LST has a statistically significant correlation with WTD only in June, July and August. Also, we observed a statistically significant moderate correlation (R = 0.41) between LST and in-situ WTD for the whole vegetation period (**Article I**).
- A general inapplicability of both TOTRAM scenarios for the spatial and temporal monitoring of in-situ WTD in northern peatlands (**Article II**).
- OPTRAM sensitivity to WTD in peatlands highly depends on vegetation cover that dominant within OPTRAM pixel. The maximum temporal Pearson correlation coefficients (R = 0.56–0.74, an average of 0.7) between in-situ WTD and OPTRAM based on Landsat_30m were observed for pixels with dominantly hollows and lawns covered with mosses and graminoids with little or no shrubs or trees (**Article II** and **Article IV**).
- There is a high potential of OPTRAM for monitoring temporal changes in WTD in both types of peatlands: bogs and fens. However, OPTRAM performance is worse in FI_LOM site, which is a peatland with a very high (often above the surface) and stable WTD (**Article IV**).
- The spatial resolution of remotely sensed data used for OPTRAM estimation can critically affect the OPTRAM performance; the best performance of OPTRAM for in-situ WTD monitoring was obtained with data of high spatial resolution – Landsat_30m (**Article IV**).
- Either WTD measured in-situ or modelled with PEATCLSM can be used to detect 'best' OPTRAM pixels, allowing for subsequent near real-time WTD monitoring using OPTRAM (**Article IV**).
- OPTRAM and PEATCLSM WTD yielded in comparable high correlation metrices with in-situ WTD **(Article III** and **Article IV**). It is suggested to assimilate OPTRAM to PEATCLSM with the purpose to contribute independent information of peat moisture information at high spatial resolution.

REFERENCES

Alm J, Schulman L, Walden J, Nykanen H, Martikainen PJ, Silvola J (1999) Carbon Balance of a Boreal Bog during a Year with an Exceptionally Dry Summer. Ecology 80:161. https://doi.org/10.2307/176987

Ambrosone M, Matese A, Di Gennaro SF, Gioli B, Tudoroiu M, Genesio L, Miglietta F, Baronti S, Maienza A, Ungaro F, Toscano P (2020) Retrieving soil moisture in rainfed and irrigated fields using Sentinel-2 observations and a modified OPTRAM approach. Int J Appl Earth Obs Geoinf 89:102113. https://doi.org/10.1016/j.jag.2020.102113

Arens M (2017) The effect of spatial organization of peatland patterns on the hydrology. Wageningen University

Arroyo-Mora JP, Kalacska M, Soffer RJ, Moore TR, Roulet NT, Juutinen S, Ifimov G, Leblanc G, Inamdar D, Arroyo-Mora JP, Kalacska M, Soffer RJ, Moore TR, Roulet NT, Juutinen S, Ifimov G, Leblanc G, Inamdar D (2018) Airborne Hyperspectral Evaluation of Maximum Gross Photosynthesis, Gravimetric Water Content, and CO2 Uptake Efficiency of the Mer Bleue Ombrotrophic Peatland. Remote Sens 10:565. https://doi.org/10.3390/rs10040565

Aurela M, Lohila A, Tuovinen J-P, Hatakka J, Laurila T, Riutta T (2009) Carbon dioxide exchange on a northern boreal fen. J Name Boreal Environ Res 14:699–710

Aurela M, Lohila A, Tuovinen J-P, Hatakka J, Penttilä T, Laurila T (2015) Carbon dioxide and energy flux measurements in four northern-boreal ecosystems at Pallas. Boreal Environ Res

Babaeian E, Sadeghi M, Franz TE, Jones S, Tuller M (2018) Mapping soil moisture with the OPtical TRApezoid Model (OPTRAM) based on long-term MODIS observations. Remote Sens Environ 211:425–440. https://doi.org/10.1016/j.rse.2018.04.029

Bechtold M, De Lannoy G, Koster RD, Reichle RH, Mahanama S, Bleuten W, Bourgault MA, Brümmer C, Burdun I, Desai AR, Devito K, Grünwald T, Grygoruk M, Humphreys ER, Klatt J, Kurbatova J, Lohila A, Munir TM, Nilsson MB, Price JS, Röhl M, Schneider A, Tiemeyer B (2019a) PEAT-CLSM: A Specific Treatment of Peatland Hydrology in the NASA Catchment Land Surface Model. J Adv Model Earth Syst 2018MS001574. https://doi.org/10.1029/2018MS001574

Bechtold M, De Lannoy G, Reichle RH (2019b) PEAT-CLSM simulation output (Northern Peatlands) version 1

Bechtold M, De Lannoy G, Reichle RH, Roose D, Balliston N, Burdun I, Devito K, Kurbatova J, Munir TM, Zarov EA (2020) Improved Groundwater Table and L-band Brightness Temperature Estimates for Northern Hemisphere Peatlands Using New Model Physics and SMOS Observations in a Global Data Assimilation Framework. Remote Sens Environ 246

Bechtold M, Schlaffer S, Tiemeyer B, De Lannoy G (2018) Inferring Water Table Depth Dynamics from ENVISAT-ASAR C-Band Backscatter over a Range of Peatlands from Deeply-Drained to Natural Conditions. Remote Sens 10:536. https://doi.org/10.3390/rs10040536

Bourgeau-Chavez LL, Kasischke ES, Riordan K, Brunzell S, Nolan M, Hyer E, Slawski J, Medvecz M, Walters T, Ames S (2007) Remote monitoring of spatial and temporal surface soil moisture in fire disturbed boreal forest ecosystems with ERS SAR imagery. Int J Remote Sens 28:2133–2162. https://doi.org/10.1080/01431160600976061

Burnett C, Aaviksoo K, Lang S, Langanke T, Blaschke T (2003) An Object-based Methodology for Mapping Mires Using High Resolution Imagery. In: Ecohydrological Processes in Northern Wetlands: Selected Papers of International Conference & Educational Workshop. Tartu University Press, Tallinn, pp 239–244

Capodici F, Cammalleri C, Francipane A, Ciraolo G, La Loggia G, Maltese A (2020) Soil Water Content Diachronic Mapping: An FFT Frequency Analysis of a Temperature–Vegetation Index. Geosciences 10:23. https://doi.org/10.3390/geosciences10010023

Carlson T (2007) An Overview of the "Triangle Method" for Estimating Surface Evapotranspiration and Soil Moisture from Satellite Imagery. Sensors 7:1612–1629. https://doi.org/10.3390/s7081612

Carlson T, Gillies R, Perry E (1994) A method to make use of thermal infrared temperature and NDVI measurements to infer surface soil water content and fractional vegetation cover. Remote Sens Rev 9:161–173. https://doi.org/10.1080/02757259409532220

Carlson TN, Petropoulos GP (2019) A new method for estimating of evapotranspiration and surface soil moisture from optical and thermal infrared measurements: the simplified triangle. Int J Remote Sens 40:7716–7729. https://doi.org/10.1080/01431161.2019.1601288

Chen M, Zhang Y, Yao Y, Lu J, Pu X, Hu T, Wang P (2020) Evaluation of an OPtical TRApezoid Model (OPTRAM) to retrieve soil moisture in the Sanjiang Plain of Northeast China. Earth Sp Sci. https://doi.org/10.1029/2020EA001108

Cox PM, Betts RA, Jones CD, Spall SA, Totterdell IJ (2000) Acceleration of global warming due to carbon-cycle feedbacks in a coupled climate model. Nature 408:184–187. https://doi.org/10.1038/35041539

Damman AWH (1996) Peat accumulation in fens and bogs: effects of hydrology and fertility. North peatlands Glob Clim Chang 213–222

De Lannoy GJM, Reichle RH (2016) Global assimilation of multiangle and multipolarization SMOS brightness temperature observations into the GEOS-5 catchment land surface model for soil moisture estimation. J Hydrometeorol 17:669–691. https://doi.org/10.1175/JHM-D-15-0037.1

Dorigo W, Wagner W, Albergel C, Albrecht F, Balsamo G, Brocca L, Chung D, Ertl M, Forkel M, Gruber A, Haas E, Hamer PD, Hirschi M, Ikonen J, de Jeu R, Kidd R, Lahoz W, Liu YY, Miralles D, Mistelbauer T, Nicolai-Shaw N, Parinussa R, Pratola C, Reimer C, van der Schalie R, Seneviratne SI, Smolander T, Lecomte P (2017) ESA CCI Soil Moisture for improved Earth system understanding: State-of-the art and future directions. Remote Sens Environ 203:185–215. https://doi.org/10.1016/j.rse.2017.07.001

Dorrepaal E, Toet S, Van Logtestijn RSP, Swart E, Van De Weg MJ, Callaghan T V., Aerts R (2009) Carbon respiration from subsurface peat accelerated by climate warming in the subarctic. Nature 460:616–619. https://doi.org/10.1038/nature08216

DuBois S, Desai AR, Singh A, Serbin SP, Goulden ML, Baldocchi DD, Ma S, Oechel WC, Wharton S, Kruger EL, Townsend PA (2018) Using imaging spectroscopy to detect variation in terrestrial ecosystem productivity across a water-stressed landscape. Ecol Appl 28:1313–1324. https://doi.org/10.1002/eap.1733

Ducharne A, Koster RD, Suarez MJ, Stieglitz M, Kumar P (2000) A catchment-based approach to modeling land surface processes in a general circulation model 2. Parameter estimation and model demonstration. J Geophys Res Atmos 105:24823–24838. https://doi.org/10.1029/2000JD900328

El Hajj M, Baghdadi N, Zribi M, Bazzi H, El Hajj M, Baghdadi N, Zribi M, Bazzi H (2017) Synergic Use of Sentinel-1 and Sentinel-2 Images for Operational Soil Moisture Mapping at High Spatial Resolution over Agricultural Areas. Remote Sens 9:1292. https://doi.org/10.3390/rs9121292

Entekhabi D, Njoku EG, O'Neill PE, Kellogg KH, Crow WT, Edelstein WN, Entin JK, Goodman SD, Jackson TJ, Johnson J, Kimball J, Piepmeier JR, Koster RD, Martin N, McDonald KC, Moghaddam M, Moran S, Reichle R, Shi JC, Spencer MW, Thurman SW, Tsang L, Van Zyl J (2010) The soil moisture active passive (SMAP) mission. Proc IEEE 98:704–716. https://doi.org/10.1109/JPROC.2010.2043918

Estonian Land Board (2020) Download Topographic Data. https://geoportaal.maaamet.ee/index.php?lang_id=2&page_id=618. Accessed 21 Feb 2020

Estonian Land Board (2019) Orthophotos. https://geoportaal.maaamet.ee/index.php?page_id=309&lang_id=2. Accessed 2 Jul 2020

Frolking S, Roulet NT (2007) Holocene radiative forcing impact of northern peatland carbon accumulation and methane emissions. Glob Chang Biol 13:1079–1088. https://doi.org/10.1111/j.1365-2486.2007.01339.x

Frolking S, Talbot J, Jones MC, Treat CC, Kauffman JB, Tuittila E-S, Roulet N (2011) Peatlands in the Earth's 21st century climate system. Environ Rev 19:371–396. https://doi.org/10.1139/a11-014

Garcia M, Fernández N, Villagarcía L, Domingo F, Puigdefábregas J, Sandholt I (2014) Accuracy of the Temperature-Vegetation Dryness Index using MODIS under water-limited vs. energy-limited evapotranspiration conditions. Remote Sens Environ 149:100–117. https://doi.org/10.1016/j.rse.2014.04.002

Gillies RR, Carlson TN, Gillies RR, Carlson TN (1995) Thermal Remote Sensing of Surface Soil Water Content with Partial Vegetation Cover for Incorporation into Climate Models. http://dx.doi.org/101175/1520-0450(1995)034<0745:TRSOSS>20CO;2. https://doi.org/10.1175/1520-0450(1995)034<0745:TRSOSS>2.0.CO;2

Gorelick N, Hancher M, Dixon M, Ilyushchenko S, Thau D, Moore R (2017) Google Earth Engine: Planetary-scale geospatial analysis for everyone. Remote Sens Environ 202:18–27. https://doi.org/10.1016/j.rse.2017.06.031

Goward SN, Cruickshanks GD, Hope AS (1985) Observed relation between thermal emission and reflected spectral radiance of a complex vegetated landscape. Remote Sens Environ 18:137–146. https://doi.org/10.1016/0034-4257(85)90044-6

Goward SN, Xue Y, Czajkowski KP (2002) Evaluating land surface moisture conditions from the remotely sensed temperature/vegetation index measurements: An exploration with the simplified simple biosphere model. Remote Sens Environ 79:225–242. https://doi.org/10.1016/S0034-4257(01)00275-9

Günther A, Barthelmes A, Huth V, Joosten H, Jurasinski G, Koebsch F, Couwenberg J (2020) Prompt rewetting of drained peatlands reduces climate warming despite methane emissions. Nat Commun 11:1–5. https://doi.org/10.1038/s41467-020-15499-z

Harris A (2008) Spectral reflectance and photosynthetic properties of Sphagnum mosses exposed to progressive drought. Ecohydrology 1:35–42. https://doi.org/10.1002/eco.5

Harris A, Bryant RG, Baird AJ (2005) Detecting near-surface moisture stress in Sphagnum spp. Remote Sens Environ 97:371–381. https://doi.org/10.1016/J.RSE.2005.05.001

Hersbach H, Bell B, Berrisford P, Hirahara S, Horányi A, Muñoz-Sabater J, Nicolas J, Peubey C, Radu R, Schepers D, Simmons A, Soci C, Abdalla S, Abellan X, Balsamo G, Bechtold P, Biavati G, Bidlot J, Bonavita M, Chiara G, Dahlgren P, Dee D, Diamantakis M, Dragani R, Flemming J, Forbes R, Fuentes M, Geer A, Haimberger L, Healy S, Hogan RJ, Hólm E, Janisková M, Keeley S, Laloyaux P, Lopez P, Lupu C, Radnoti G, Rosnay P, Rozum I, Vamborg F, Villaume S, Thépaut J (2020) The ERA5 Global Reanalysis. Q J R Meteorol Soc 1–51. https://doi.org/10.1002/qj.3803

Holzman ME, Rivas R, Piccolo MC (2014) Estimating soil moisture and the relationship with crop yield using surface temperature and vegetation index. Int J Appl Earth Obs Geoinf 28:181–192. https://doi.org/10.1016/J.JAG.2013.12.006

Hooijer A, Page S, Jauhiainen J, Lee WA, Lu XX, Idris A, Anshari G (2012) Subsidence and carbon loss in drained tropical peatlands. Biogeosciences 9:1053–1071. https://doi.org/10.5194/bg-9-1053-2012

Huang F, Wang P, Ren Y, Liu R (2019) Estimating Soil Moisture Using the Optical Trapezoid Model (OPTRAM) in a Semi-Arid Area of SONGNEN Plain, China Based on Landsat-8 Data. In: International Geoscience and Remote Sensing Symposium (IGARSS). Institute of Electrical and Electronics Engineers Inc., Yokohama, Japan, pp 7010–7013

ICOS (2018) Degerö Vegetation. https://www.icos-sweden.se/station_degero.html

Ivanov KE (1981) Water movement in Mirelands. London: Academic Press

Jackson TJ, Chen D, Cosh M, Li F, Anderson M, Walthall C, Doriaswamy P, Hunt ER (2004) Vegetation water content mapping using Landsat data derived normalized difference water index for corn and soybeans. In: Remote Sensing of Environment. Elsevier, pp 475–482

Kalacska M, Arroyo-Mora J, de Gea J, Snirer E, Herzog C, Moore T (2013) Videographic Analysis of Eriophorum Vaginatum Spatial Coverage in an Ombotrophic Bog. Remote Sens 5:6501–6512. https://doi.org/10.3390/rs5126501

Karnieli A, Agam N, Pinker RT, Anderson M, Imhoff ML, Gutman GG, Panov N, Goldberg A (2010) Use of NDVI and Land Surface Temperature for Drought Assessment: Merits and Limitations. J Clim 23:618–633. https://doi.org/10.1175/2009JCLI2900.1

Kellner E, Halldin S (2002) Water budget and surface-layer water storage in a Sphagnum bog in central Sweden. Hydrol Process 16:87–103. https://doi.org/10.1002/hyp.286

Kerr YH, Waldteufel P, Wigneron JP, Delwart S, Cabot F, Boutin J, Escorihuela MJ, Font J, Reul N, Gruhier C, Juglea SE, Drinkwater MR, Hahne A, Martin-Neira M, Mecklenburg S (2010) The SMOS L: New tool for monitoring key elements ofthe global water cycle. Proc IEEE 98:666–687. https://doi.org/10.1109/JPROC.2010.2043032

Keskkonnaagentuur (2002) Maastike kaugseire 2002. Tallinn

Koster RD, Suarez MJ, Ducharne A, Stieglitz M, Kumar P (2000) A catchment-based approach to modeling land surface processes in a general circulation model 1. Model structure. J Geophys Res Atmos 105:24809–24822. https://doi.org/10.1029/2000JD900327

Kull A, Kull A, Jaagus J, Kuusemets V, Mander Ü (2008) The effects of fluctuating climatic conditions and weather events on nutrient dynamics in a narrow mosaic riparian peatland. Boreal Environ Res 13:243–263

Lafleur PM, Hember RA, Admiral SW, Roulet NT (2005a) Annual and seasonal variability in evapotranspiration and water table at a shrub-covered bog in southern Ontario, Canada. Hydrol Process 19:3533–3550. https://doi.org/10.1002/hyp.5842

Lafleur PM, Moore TR, Roulet NT, Frolking S (2005b) Ecosystem Respiration in a Cool Temperate Bog Depends on Peat Temperature But Not Water Table. Ecosystems 8:619–629. https://doi.org/10.1007/s10021-003-0131-2

Letendre J, Poulin M, Rochefort L (2008) Sensitivity of spectral indices to CO2 fluxes for several plant communities in a Sphagnum-dominated peatland. Can J Remote Sens 34:S414–S425. https://doi.org/10.5589/m08-053

Li J, Chen W, Touzi R (2007) Optimum RADARSAT-1 configurations for wetlands discrimination: A case study of the Mer Bleue peat bog. Can J Remote Sens 33:S46–S55. https://doi.org/10.5589/m07-046

Limpens J, Berendse F, Blodau C, Canadell JG, Freeman C, Holden J, Roulet N, Rydin H, Schaepman-Strub G (2008) Peatlands and the carbon cycle: from local processes to global implications – a synthesis. Biogeosciences 5:1475–1491. https://doi.org/10.5194/bg-5-1475-2008

Lindholm T, Markkula I (1984) Moisture conditions in hummocks and hollows in virgin and drained sites on the raised bog Laaviosuo, southern Finland. Ann Bot Fenn 21:241–255

Lode E, Küttim M, Kiivit IK (2017) Indicative effects of climate change on groundwater levels in estonian raised bogs over 50 years. Mires Peat 19. https://doi.org/10.19189/MaP.2016.OMB.255

Long D, Singh VP (2012) A Two-source Trapezoid Model for Evapotranspiration (TTME) from satellite imagery. Remote Sens Environ 121:370–388. https://doi.org/10.1016/j.rse.2012.02.015

Mallick K, Bhattacharya BK, Patel NK (2009) Estimating volumetric surface moisture content for cropped soils using a soil wetness index based on surface temperature and NDVI. Agric For Meteorol 149:1327–1342. https://doi.org/10.1016/j.agrformet.2009.03.004

Mananze S, Pôças I (2019) Agricultural drought monitoring based on soil moisture derived from the optical trapezoid model in Mozambique. J Appl Remote Sens 13:1. https://doi.org/10.1117/1.jrs.13.024519

McVicar TR, Roderick ML, Donohue RJ, Li LT, Van Niel TG, Thomas A, Grieser J, Jhajharia D, Himri Y, Mahowald NM, Mescherskaya A V., Kruger AC, Rehman S, Dinpashoh Y (2012) Global review and synthesis of trends in observed terrestrial near-surface wind speeds: Implications for evaporation. J. Hydrol. 416–417:182–205

Moore TR, Knowles R (1989) The influence of water table levels on methane and carbon dioxide emissions from peatland soils. Can J Soil Sci 69:33–38. https://doi.org/10.4141/cjss89-004

Moran MSS, Clarke TRR, Inoue Y, Vidal A (1994) Estimating crop water deficit using the relation between surface-air temperature and spectral vegetation index. Remote Sens Environ 49:246–263. https://doi.org/10.1016/0034-4257(94)90020-5

Myhre G, Shindell D, Bréon FM, Collins W, Fuglestvedt J, Huang J, Koch D, Lamarque JF, Lee D, Mendoza B (2013) Climate change 2013: the physical science basis. Contrib Work Gr I to fifth Assess Rep Intergov panel Clim Chang 659–740

Nemani R, Pierce L, Running S, Goward S, Nemani R, Pierce L, Running S, Goward S (1993) Developing Satellite-derived Estimates of Surface Moisture Status. J Appl Meteorol. https://doi.org/10.1175/1520-0450(1993)032<0548:DSDEOS>2.0.CO;2

Nijp JJ, Metselaar K, Limpens J, Bartholomeus HM, Nilsson MB, Berendse F, van der Zee SEATM (2019) High-resolution peat volume change in a northern peatland: Spatial variability, main drivers, and impact on ecohydrology. Ecohydrology 12:. https://doi.org/10.1002/eco.2114

Osterwalder S, Sommar J, Åkerblom S, Jocher G, Fritsche J, Nilsson MB, Bishop K, Alewell C (2018) Comparative study of elemental mercury flux measurement techniques over a Fennoscandian boreal peatland. Atmos Environ 172:16–25. https://doi.org/10.1016/j.atmosenv.2017.10.025

Paal J, Leibak E (2011) Estonian mires: inventory of habitats. Estimaa Looduse Fond, Tartu

Pärn J, Verhoeven JTA, Butterbach-Bahl K, Dise NB, Ullah S, Aasa A, Egorov S, Espenberg M, Järveoja J, Jauhiainen J, Kasak K, Klemedtsson L, Kull A, Laggoun-Défarge F, Lapshina ED, Lohila A, Lõhmus K, Maddison M, Mitsch WJ, Müller C, Niinemets Ü, Osborne B, Pae T, Salm J-O, Sgouridis F, Sohar K, Soosaar K, Storey K, Teemusk A, Tenywa MM, Tournebize J, Truu J, Veber G, Villa JA, Zaw SS, Mander Ü (2018) Nitrogen-rich organic soils under warm well-drained conditions are global nitrous oxide emission hotspots. Nat Commun 9:1135. https://doi.org/10.1038/s41467-018-03540-1

Patel NR, Anapashsha R, Kumar S, Saha SK, Dadhwal VK (2009) Assessing potential of MODIS derived temperature/vegetation condition index (TVDI) to infer soil moisture status. Int J Remote Sens 30:23–39. https://doi.org/10.1080/01431160802108497

Peichl M, Sagerfors J, Lindroth A, Buffam I, Grelle A, Klemedtsson L, Laudon H, Nilsson MB (2013) Energy exchange and water budget partitioning in a boreal minerogenic mire. J Geophys Res Biogeosciences 118:1–13. https://doi.org/10.1029/2012JG002073

Péli ER, Nagy J, Cserhalmi D (2015) In Situ measurements of seasonal productivity dynamics in two Sphagnum dominated mires in Hungary. Carpathian J Earth Environ Sci 10:231–240

Post WM, Emanuel WR, Zinke PJ, Stangenberger AG (1982) Soil carbon pools and world life zones. Nature 298:156–159. https://doi.org/10.1038/298156a0

Price J (1997) Soil moisture, water tension, and water table relationships in a managed cutover bog. J Hydrol 202:21–32. https://doi.org/10.1016/S0022-1694(97)00037-1

Price JC (1990) Using Spatial Context in Satellite Data to Infer Regional Scale Evapotranspiration. IEEE Trans Geosci Remote Sens 28:940–948. https://doi.org/10.1109/36.58983

Price JS, Schlotzhauer SM (1999) Importance of shrinkage and compression in determining water storage changes in peat: the case of a mined peatland. Hydrol Process 13:2591–2601. https://doi.org/10.1002/(SICI)1099-1085(199911)13:16<2591::AID-HYP933>3.0.CO;2-E

Prihodko L, Goward SN (1997) Estimation of air temperature from remotely sensed surface observations. Remote Sens Environ 60:335–346. https://doi.org/10.1016/S0034-4257(96)00216-7

R Core Team (2018) R: A Language and Environment for Statistical Computing

Räsänen A, Aurela M, Juutinen S, Kumpula T, Lohila A, Penttilä T, Virtanen T (2019) Detecting northern peatland vegetation patterns at ultra-high spatial resolution. Remote Sens Ecol Conserv rse2.140. https://doi.org/10.1002/rse2.140

Rosenberry DO, Glaser PH, Siegel DI, Weeks EP (2003) Use of hydraulic head to estimate volumetric gas content and ebullition flux in northern peatlands. Water Resour Res 39:. https://doi.org/10.1029/2002WR001377

Roulet NT, Lafleur PM, Richard PJH, Moore TR, Humphreys ER, Bubier J (2007) Contemporary carbon balance and late Holocene carbon accumulation in a northern peatland. Glob Chang Biol 13:397–411. https://doi.org/10.1111/j.1365-2486.2006.01292.x

Sadeghi M, Babaeian E, Tuller M, Jones SB (2017) The optical trapezoid model: A novel approach to remote sensing of soil moisture applied to Sentinel-2 and Landsat-8 observations. Remote Sens Environ 198:52–68. https://doi.org/10.1016/J.RSE.2017.05.041

Sadeghi M, Jones SB, Philpot WD (2015) A linear physically-based model for remote sensing of soil moisture using short wave infrared bands. Remote Sens Environ 164:66–76. https://doi.org/10.1016/j.rse.2015.04.007

Salm J-O, Maddison M, Tammik S, Soosaar K, Truu J, Mander Ü (2012) Emissions of CO2, CH4 and N2O from undisturbed, drained and mined peatlands in Estonia. Hydrobiologia 692:41–55. https://doi.org/10.1007/s10750-011-0934-7

Sandholt I, Rasmussen K, Andersen J (2002) A simple interpretation of the surface temperature/vegetation index space for assessment of surface moisture status. Remote Sens Environ 79:213–224. https://doi.org/10.1016/S0034-4257(01)00274-7

Scharlemann JPW, Tanner EVJ, Hiederer R, Kapos V (2014) Global soil carbon: Understanding and managing the largest terrestrial carbon pool. Carbon Manag 5:81–91. https://doi.org/10.4155/cmt.13.77

Serbin SP, Singh A, Desai AR, Dubois SG, Jablonski AD, Kingdon CC, Kruger EL, Townsend PA (2015) Remotely estimating photosynthetic capacity, and its response to temperature, in vegetation canopies using imaging spectroscopy. Remote Sens Environ 167:78–87. https://doi.org/10.1016/j.rse.2015.05.024

Sillasoo U, Mauquoy D, Blundell A, Charman D, Blaauw M, Daniell JRG, Toms P, Newberry J, Chambers FM, Karofeld E (2007) Peat multi-proxy data from Männikjärve bog as indicators of late Holocene climate changes in Estonia. Boreas 36:20–37. https://doi.org/10.1111/j.1502-3885.2007.tb01177.x

Sonnentag O, Chen JM, Roberts DA, Talbot J, Halligan KQ, Govind A (2007) Mapping tree and shrub leaf area indices in an ombrotrophic peatland through multiple endmember spectral unmixing. Remote Sens Environ 109:342–360. https://doi.org/10.1016/j.rse.2007.01.010

Strack M, Price JS (2009) Moisture controls on carbon dioxide dynamics of peat-Sphagnum monoliths. Ecohydrology 2:34–41. https://doi.org/10.1002/eco.36

Strilesky SL, Humphreys ER (2012) A comparison of the net ecosystem exchange of carbon dioxide and evapotranspiration for treed and open portions of a temperate peatland. Agric For Meteorol 153:45–53. https://doi.org/10.1016/j.agrformet.2011.06.006

Sulman BN, Desai AR, Cook BD, Saliendra N, Mackay DS (2009) Contrasting carbon dioxide fluxes between a drying shrub wetland in Northern Wisconsin, USA, and nearby forests. Biogeosciences 6:1115–1126. https://doi.org/10.5194/bg-6-1115-2009

Swindles GT, Morris PJ, Mullan DJ, Payne RJ, Roland TP, Amesbury MJ, Lamentowicz M, Turner TE, Gallego-Sala A, Sim T, Barr ID, Blaauw M, Blundell A, Chambers FM, Charman DJ, Feurdean A, Galloway JM, Gałka M, Green SM, Kajukało K, Karofeld E, Korhola A, Lamentowicz Ł, Langdon P, Marcisz K, Mauquoy D, Mazei YA, McKeown MM, Mitchell EAD, Novenko E, Plunkett G, Roe HM, Schoning K, Sillasoo Ü, Tsyganov AN, van der Linden M, Väliranta M, Warner B (2019) Widespread drying of European peatlands in recent centuries. Nat Geosci 12:922–928. https://doi.org/10.1038/s41561-019-0462-z

Talbot J, Richard PJH, Roulet NT, Booth RK (2010) Assessing long-term hydrological and ecological responses to drainage in a raised bog using paleoecology and a hydrosequence. J Veg Sci 21:143–156. https://doi.org/10.1111/j.1654-1103.2009.01128.x

Tang R, Li Z-L, Tang B (2010) An application of the Ts–VI triangle method with enhanced edges determination for evapotranspiration estimation from MODIS data in arid and semi-arid regions: Implementation and validation. Remote Sens Environ 114:540–551. https://doi.org/10.1016/J.RSE.2009.10.012

Torres R, Snoeij P, Geudtner D, Bibby D, Davidson M, Attema E, Potin P, Rommen BÖ, Floury N, Brown M, Traver IN, Deghaye P, Duesmann B, Rosich B, Miranda N, Bruno C, L'Abbate M, Croci R, Pietropaolo A, Huchler M, Rostan F (2012) GMES Sentinel-1 mission. Remote Sens Environ 120:9–24. https://doi.org/10.1016/j.rse.2011.05.028

Ulaby F, Long D (2014) Microwave radar and radiometric remote sensing. University of Michigan Press, Michigan, USA

Ulaby FT, Moore RK, Fung AK (1981) Microwave remote sensing: Active and Passive. Artech House, Massachusetts

Wagner W, Lemoine G, Borgeaud M, Rott H (1999) A study of vegetation cover effects on ers scatterometer data. IEEE Trans Geosci Remote Sens 37:938–948. https://doi.org/10.1109/36.752212

Wang W, Huang D, Wang X-G, Liu Y-R, Zhou F (2011) Hydrology and Earth System Sciences Estimation of soil moisture using trapezoidal relationship between remotely sensed land surface temperature and vegetation index. Hydrol Earth Syst Sci 15:1699–1712. https://doi.org/10.5194/hess-15-1699-2011

Xu J, Morris PJ, Liu J, Holden J (2018) PEATMAP: Refining estimates of global peatland distribution based on a meta-analysis. Catena 160:134–140. https://doi.org/10.1016/j.catena.2017.09.010

Yu Z (2011) Holocene carbon flux histories of the world's peatlands. The Holocene 21:761–774. https://doi.org/10.1177/0959683610386982

Yu Z, Beilman DW, Frolking S, MacDonald GM, Roulet NT, Camill P, Charman DJ (2011) Peatlands and Their Role in the Global Carbon Cycle. Eos, Trans Am Geophys Union 92:97–98. https://doi.org/10.1029/2011EO120001

Yu Z, Loisel J, Brosseau DP, Beilman DW, Hunt SJ (2010) Global peatland dynamics since the Last Glacial Maximum. Geophys Res Lett 37:. https://doi.org/10.1029/2010GL043584

Zhang D, Tang R, Tang BH, Wu H, Li ZL (2015) A simple method for soil moisture determination from LST-VI feature space using nonlinear interpolation based on thermal infrared remotely sensed data. IEEE J Sel Top Appl Earth Obs Remote Sens 8:638–648. https://doi.org/10.1109/JSTARS.2014.2371135

Zhang D, Tang R, Zhao W, Tang B, Wu H, Shao K, Li Z-L (2014) Surface Soil Water Content Estimation from Thermal Remote Sensing based on the Temporal Variation of Land Surface Temperature. Remote Sens 6:3170–3187. https://doi.org/10.3390/rs6043170

Zhang R, Tian J, Su H, Sun X, Chen S, Xia J (2008) Two Improvements of an Operational Two-Layer Model for Terrestrial Surface Heat Flux Retrieval. Sensors 8:6165–6187. https://doi.org/10.3390/s8106165

Zwieback S, Berg AA (2019) Fine-Scale SAR Soil Moisture Estimation in the Subarctic Tundra. IEEE Trans Geosci Remote Sens 57:4898–4912. https://doi.org/10.1109/TGRS.2019.2893908

(2019) Wiscland 2 Land Cover Database

SUMMARY IN ESTONIAN

Põhjapoolkera soode põhjaveetaseme seire täiendamine optiliste ja termiliste satelliidiandmete abil

Doktoritöö eesmärgiks on arendada optilise ja termilise satelliitkaugseire andmestiku põhjal boreaalsete märgalade veetaseme ajalise muutlikkuse seire võimalusi. Töös keskendutakse kitsamalt kaugseire termokanalitest teisendatud maapinna temperatuurile (LST) ja lühi-infrapunase spektrikanali (SWIR) andmetele ning nendel põhinevatele TOTRAM ja OPTRAM mudelitele, et hinnata nende sobivust veetaseme seiramiseks.

Publikatsioonis I hinnati LST andmete rakendatavust hüdrometeoroloogiliste tingimuste (sealhulgas ka veetaseme) jälgimiseks Eesti soodes. Kasutasime MODIS platvormi LST ja Männikjärve raba (Eesti) kohapeal mõõdetud hüdrometeoroloogilisi andmeid, mis hõlmasid 2008–2016 aastate vegetatsiooniperioode (maist-septembrini). Selle põhjal järeldasime, et LST ajaline muutlikkus on veetasemega mõõdukalt seotud (R = 0.35–0.5 statistiliselt oluliselt).

Soo veerežiimi ajalis-ruumilise käigu kirjeldamiseks katsetasime kahte trapetsoidil põhinevat mudelit: TOTRAM mudel põhineb optilistest kanalitest arvutatud vegetatsiooniindeksi ja maapinna temperatuuri (LST) teljestiku kasutamisel, OPTRAM mudel põhineb aga ainult optilistel andmetel ja kasutab vegetatsiooniindeksi ning infrapuna lühilaine peegeldumise STR (Shortwave infrared Transformed Reflectance) teljestikku. Mõlemat mudelit kasutati veetaseme ajalis-ruumilise dünaamika hindamiseks Männikjärve rabas ja Linnusaare soos. Tulemused näitasid, et TOTRAM mudel ei ole boreaalsetes rabades veetaseme seireks rakendatav. Seevastu OPTRAM mudelil on edasistes uuringutes veetaseme ajaliste muutuste hindamiseks suur potentsiaal.

Töös esitatakse NASA Goddard instituudi maavaatlussüsteemi (GEOS) loodud valgla maapinnamudeli (Catchment Land Surface Model – CLSM) märgaladele kohandatud valgla maapinna hüdroloogia moodul (PEATCLSM). See moodul kasutab CLSM-i põhistruktuuri, mida on täiendatud kirjandusest pärit turvasmuldadele omaste parameetritega. Simulatsioonis kasutasime nii CLSM kui PEATCLSM-i, mille tulemusi on võrreldud neljakümne nelja põhjapoolkera (vahemik 40°–75°N) märgala veetaseme pikaajaliste andmetega. Tulemused näitavad, et PEATCLSM suudab veetaseme muutusi paremini kirjeldada kui algne CLSM, mistõttu edasises töös kasutati kasutati PEATCLSM mudelit.

PEATCLSM arvutuste tulemusi kasutati sisendina publikatsioonis IV, kus analüüsiti OPTRAM mudeli kasutatavust veetaseme dünaamika kirjeldamiseks viiel pikaajaliste (üle 10 aastat) kohapealsete vaatlusandmetega märgaladel Eestis, Soomes, Kanadas ja USAs, mis hõlmasid nii rabasid kui madalsoid. Pakkusime lähenemisviisi nn lokaalsete esinduslike OPTRAM-pikslite valimiseks, mis on eeldatavasti veetaseme muutuse suhtes kõige tundlikumad. Järeldati, et OPTRAM-i tundlikkus veetaseme suhtes sõltub suuresti valitud piksli domineerivast taimkattest. Pikslite puhul, mis asuvad älvestes või tasastel aladel, kus domineerivad

sambla-rohukooslused ning kus on hõre puhma- ja puurinne, täheldati kohapeal mõõdetud veetaseme ja OPTRAM tulemuste vahel kõige tugevamat seost (R = 0.56–0.74, keskmiselt 0.7). Lisaks leiti, et OPTRAM-i kaugseire andmete ruumiline eraldusvõime võib mudeli jõudlust kriitiliselt mõjutada. OPTRAM-i parim jõudlus saavutati 30 meetrise ruumilise eraldusvõimega Landsat andmete kasutamisel. Viimaks selgus, et lokaalsete sobilike veetaseme muutusele tundlike OPTRAM-pikslite leidmiseks võib kasutada nii kohapeal mõõdetud, kui ka PEATCLSM-iga modelleeritud veetaseme andmeid.

Kuigi uuringus kasutatud soode arv on piiratud, näitavad tulemused olulist ajalise muutlikkuse seost neil uurimisaladel ning seega võib OPTRAM mudelil põhinevat indeksit rakendada pikaajaliseks ja peaaegu reaalajaliseks veetaseme hindamiseks suures laiuskraadivahemikus paiknevatel märgaladel.

ACKNOWLEDGEMENTS

I am truly grateful to all people with whom I have shared and discussed this research. Foremost, I want to thank my supervisors Dr **Valentina Sagris** and Prof. **Ülo Mander** from the University of Tartu for continuous support, cooperation and support. Thank you for introducing me Estonian peatlands and organising fieldwork in the most picturesque peatlands I have ever seen.

My heartfelt gratitude goes to colleagues from GIS and Physical Geography departments. You taught me how to make GHG measurements, how to interpret my data and how to do the science. I am sincerely grateful to Dr **Ain Kull** for his wise pieces of advice and openness; thank you for discussing with me the results of my research, teaching me and reviewing my texts. I am really grateful to Dr **Evelyn Uuemaa** for creating a warm academic environment, formal and informal support. I would like to thank PhD students: Isaac Newton Kwasi Buo, Bruno Montibeller, Holger Virro, Thomas Schindler and others for various kinds of support.

I especially thank my co-authors Dr **Michel Bechtold** and Prof. **Gabrielle De Lannoy** from KU Leuven (Belgium) for the support you gave me and believing in me when it was a tough time in my study. I am grateful to KU Leuven team, particularly Anne Felsberg, for the wonderful time I had in Leuven.

During my PhD study, I have received Dora Plus and Kristjan Jaak scholarships for studying abroad, attending conferences and summer school. Writing this dissertation was possible thanks to the doctoral allowance from the Ministry of Education and Research of the Republic of Estonia, and University of Tartu.

Last but not least, I want to thank my family who has always been there for me. All this has not been possible without the invaluable support from my husband **Oleksand Karasov**. My deepest gratitude to you.

Thank you all!

PUBLICATIONS

CURRICULUM VITAE

Name	Iuliia Burdun
Date of birth	04.04.1993
Researcher ID	AAH-9790-2020
ORCID	0000-0002-1436-2550
E-mail	iuliia.burdun@ut.ee

Institutions and positions

18.09.2017–17.10.2017
University of Tartu, Faculty of Science and Technology (old), Institute of Ecology and Earth Sciences, Tartu University, Department of Geography, Adjunct instructor (0,10)

01.11.2014–31.12.2014
Physical Geography and Cartography Department of V. N. Karazin Kharkiv National University, Kharkiv (Ukraine), Participation in the Research project within the coordination plan of the Ministry of Education and Science of Ukraine "Development of a model of territorial organization of the Donetskside natural region based on remote sensing methods and GIS-technologies" (state registration number 0113U002427) (0,10)

Education

01.07.2019–05.07.2019
International Summer School Data FAIRness in Environmental & Earth Science Infrastructures: theory and practice

01.09.2019–28.02.2020
Individual doctoral project "Implementation and validation of the Ts-Vi triangle method for water table depth estimation from Landsat data in Northern peatlands" at the KU Leuven, Leuven, Belgium, 6 months

30.07.2018–04.08.2018
Summer school "Unmanned Vehicles in Earth Sciences", University of Tartu, Tartu, Estonia

11.06.2018–16.06.2018
Fifth International SPLIT Remote Sensing Professional Summer School 2018, Czech University of Life Sciences, Prague, Czech Republic

21.05.2018–25.05.2018
IMPRESSIONS Summer School "Exploring climate change. Challenges and solutions in the real world: from research to practice", Sofia, Bulgaria

17.09.2018–20.09.2018
Summer school of land use history, Karula NP & Tartu, Estonia

04.09.2017–08.09.2017
NOVA Phd Course "GIS-based Analysis of Ecosystem Services", University of Eastern Finland, School of Forest Sciences, Joensuu, Finland

02.03.2017–12.03.2017
Järvselja Spring School 2017 – Biological processes in the biosphere-atmosphere system

15.09.2015–15.07.2016
Individual doctoral project "Applied analysis of the man-made landscapes using GIS technology and remote sensing data" at the Department of Geography, University of Minho, Portugal, 10 months

R&D related managerial and administrative work

2020−... Member of American Geophysical Union (AGU)
2019−... Member of European Geosciences Union (EGU)

Academic degrees

Iuliia Burdun, Phd student, (sup) Valentina Sagris; Ülo Mander, Satellite-derived Land Surface Temperature (LST) as Proxy for Greenhouse Gas Fluxes in Boreal Peatlands, University of Tartu, Faculty of Science and Technology, Institute of Ecology and Earth Sciences.

Honours & awards

2019 Dora Plus short-term mobility grant: oral presentation at the General Assembly 2019 of the European Geosciences Union (EGU) in Vienna, Austria, from 7–12 April 2019
2019 Kristjan Jaak short study visit grant: poster presentation at the European Space Agency's 2019 Living Planet Symposium 13–17 May 2019 in Milan, Italy
2019 Dora Plus PhD student mobility grant: visiting PhD researcher (01.09.2019 – 28.02.2020) at the Catholic University of Leuven, Belgium
2018 Dora Plus short-term mobility grant: participation at "Fifth International SPLIT REMOTE SENSING® PROFESSIONAL SUMMER SCHOOL", 11.06.2018–15.06.2018, Prague, Czech Republic

Fields of research

ETIS CLASSIFICATION: 4. Natural Sciences and Engineering; 4.2. Geosciences; CERCS CLASSIFICATION: P510 Physical geography, geomorphology, pedology, cartography, climatology

Projects in progress

MOBERC20 “Estimating N2O Budgets in Organic soils – from Local to Global Scale (N2ORG) (1.05.2019–30.11.2020)”, Ülo Mander, University of Tartu, Faculty of Science and Technology, Institute of Ecology and Earth Sciences.

Supervised dissertations

Isaac Newton Kwasi Buo, Master’s Degree, 2019, (sup) Valentina Sagris; Iuliia Burdun, Urban sprawl dynamics and Urban Heat Islands (UHI) in Ghana, University of Tartu, Faculty of Science and Technology, Institute of Ecology and Earth Sciences.

Publications

2020

Bechtold, M.; De Lannoy, G.; Reichle, R. H.; Roose, D.; Balliston, N.; Burdun, I.; Devito, K.; Kurbatova, J.; Munir, T. M.; Zarov, E. A. (2020). Improved Groundwater Table and L-band Brightness Temperature Estimates for Northern Hemisphere Peatlands Using New Model Physics and SMOS Observations in a Global Data Assimilation Framework. Remote Sensing of Environment.10.1016/j.rse.2020.111805.

Burdun, Iuliia; Bechtold, Michel; Sagris, Valentina; Komisarenko, Viacheslav; De Lannoy, Gabrielle; Mander, Ülo (2020). A Comparison of Three Trapezoid Models Using Optical and Thermal Satellite Imagery for Water Table Depth Monitoring in Estonian Bogs. Remote Sensing, 12 (12), 1980.10.3390/rs12121980.

Burdun, Iuliia; Sagris, Valentina; Bechtold, Michel; Komisarenko, Viacheslav; Mander, Ülo; De Lannoy, Gabrielle (2020). Evaluation of Satellite-Based Optical and Thermal Trapezoid Methods for Groundwater Table Depth Monitoring in Estonian Bogs. *EGU General Assembly 2020.* European Geosciences Union. 10.5194/egusphere-egu2020-10544.

Bechtold, Michel; De Lannoy, Gabrielle; Reichle, Rolf H.; Roose, Dirk; Balliston, Nicole; Burdun, Iuliia; Devito, Kevin; Kurbatova, Juliya; Strack, Maria; Zarov, Evgeny A. (2020). 10 yrs of Improved Groundwater Table Estimates in Northern Peatlands Through Assimilation of Passive Microwave Observations into PEATCLSM. *EGU General Assembly 2020.* European Geosciences Union. 10.5194/egusphere-egu2020-19972.

2019

Burdun, Iuliia; Sagris, Valentina; Mander, Ülo (2019). Relationships between field-measured hydrometeorological variables and satellite-based land surface temperature in a hemiboreal raised bog. International Journal of Applied Earth Observation and Geoinformation, 74, 295−301. 10.1016/j.jag.2018.09.019.

Bechtold, M.; De Lannoy, G. J. M.; Koster, R. D.; Reichle, R. H.; Mahanama, S. P.; Bleuten, W.; Bourgault, M. A.; Brümmer, C.; Burdun, I.; Desai, A. R.; Devito, K.; Grünwald, T.; Grygoruk, M.; Humphreys, E. R.; Klatt, J.; Kurbatova, J.; Lohila, A.; Munir, T. M.; Nilsson, M. B.; Price, J. S... Tiemeyer, B. (2019). PEAT-CLSM: A Specific Treatment of Peatland Hydrology in the NASA Catchment Land Surface Model. Journal of Advances in Modeling Earth Systems, 11 (7), 2130−2162.10.1029/2018MS001574.

Karasov, Oleksandr; Külvik, Mart; Burdun, Iuliia (2019). Deconstructing landscape pattern: applications of remote sensing to physiognomic landscape mapping. Geojournal. 10.1007/s10708-019-10058-6.

Burdun, I.; Sagris,V.; Palo, A. (2019). Kuidas hinnata raba niiskust kosmosest? [How to detect moisture of bog peat from space?]. Pae, T; Mander, Ü. (Toim.). Publicationes Instituti Geographici Universitatis Tartuensis (97−105). Tartu: Tartu Ülikooli Kirjastus.

Burdun, Iuliia; Sagris, Valentina; Mander, Ülo (2019). Relationships between MODIS LST and hydrometeorological variables in a hemiboreal raised bog. *EGU2019-7166, 21: The General Assembly 2019 of the European Geosciences Union (EGU), Austria Center Vienna (ACV) in Vienna, Austria,7–12 April 2019.* Vienna: EGU General Assembly 2019. (Geophysical Research Abstracts).

Bechtold, Michel; De Lannoy, Gabrielle; Reichle, Rolf H.; Roose, Dirk; Balliston, Nicole; Burdun, Iuliia; Devito, Kevin; Grygoruk, Mateusz; Kurbatova, Juliya; Munir, Tariq M.; (2019). Assimilation of L-band Brightness Temperatures into a Global Land Surface Model to Improve Groundwater Table Estimates in Northern Peatlands. AGUFM, 2019, H33B−08.

2018

Soosaar, K., Schindler, T., Machácová, K., Krasnov, D., Burdun, I., Suija, A., Uri, V., Niinemets, Ü., Morozov, G., Mander, Ü. (2018). Flooding-induced CO2 and CH4 fluxes from an experimental grey alder forest: from ground to tree level. *Geophysical Research Abstracts, Vol. 20: EGU, Vienna, 8–13 April 2018.* Geophysical Research Abstracts: EGU General Assembly. (EGU2018-13998).

Schindler, T; Mander, Ü; Machácová, K; Burdun, I; Krasnov, D; Veber, G; Suija, A; Soosaar, K. (2018). Impact of flooding on N_2O fluxes from tree stems in a grey alder forest. *Geophysical Research Abstracts, 20: EGU General Assembly 2018.* Vienna: European Geosciences Union. (EGU2018-13486).

Mander, Ülo; Soosaar, Kaido; Burdun, Iuliia; Kännaste, Astrid; Kask, Kaia; Krasnov, Dmitrii; Krasnova, Alisa; Kriiska, Kaie; Kurvits, Tiia; Machacova, Katerina; Maddison, Martin; Morozov, Gunnar; Noe, Steffen; Ostonen, Ivika; Püssa, Kersti; Repp, Kalev; Schindler, Thomas; Suija, Ave; Veber, Gert; Niinemets, Ülo (2018). Forest ecosystem response to sudden flooding in the middle of growing season: The FluxGAF experiment. *Geophysical Research Abstracts, 20: EGU General Assembly 2018, Vienna.* Copernicus Gesellschaft Mbh.

2017

Vieira, António; Bento-Gonçalves, António; Karasov, Oleksandr; Burdun, Iuliia; Uacane, Mário; Ombe, Zacarias (2017). The Recurrence of Forest Fires in the Gorongosa National Park (Mozambique). In: António José Bento Gonçalves, António Avelino Batista Vieira, Maria Rosário Melo Costa, and José Tadeu Marques (Ed.). Wildfires: Perspectives, Issues and Challenges of the 21st Century. Nova Publishers. (Natural Disaster Research, Prediction and Mitigation).

DISSERTATIONES GEOGRAPHICAE UNIVERSITATIS TARTUENSIS

1. **Вийви Руссак.** Солнечная радиация в Тыравере. Тарту, 1991.
2. **Urmas Peterson.** Studies on Reflectance Factor Dynamics of Forest Communities in Estonia. Tartu, 1993.
3. **Ülo Suursaar.** Soome lahe avaosa ja Eesti rannikumere vee kvaliteedi analüüs. Tartu, 1993.
4. **Kiira Aaviksoo.** Application of Markov Models in Investigation of Vegetation and Land Use Dynamics in Estonian Mire Landscapes. Tartu, 1993.
5. **Kjell Weppling.** On the assessment of feasible liming strategies for acid sulphate waters in Finland. Tartu, 1997.
6. **Hannes Palang.** Landscape changes in Estonia: the past and the future. Tartu, 1998.
7. **Eiki Berg.** Estonia's northeastern periphery in politics: socio-economic and ethnic dimensions. Tartu, 1999.
8. **Valdo Kuusemets.** Nitrogen and phosphorus transformation in riparian buffer zones of agricultural landscapes in Estonia. Tartu, 1999.
9. **Kalev Sepp.** The methodology and applications of agricultural landscape monitoring in Estonia. Tartu, 1999.
10. **Rein Ahas.** Spatial and temporal variability of phenological phases in Estonia. Tartu, 1999.
11. **Эркки Таммиксаар.** Географические аспекты творчества Карла Бэра в 1830–1840 гг. Тарту, 2000.
12. **Garri Raagmaa.** Regional identity and public leaders in regional economic development. Tartu, 2000.
13. **Tiit Tammaru.** Linnastumine ja linnade kasv Eestis nõukogude aastatel. Tartu, 2001.
14. **Tõnu Mauring.** Wastewater treatment weltlands in Estonia: efficiency and landscape analysis. Tartu, 2001.
15. **Ain Kull.** Impact of weather and climatic fluctuations on nutrient flows in rural catchments. Tartu, 2001.
16. **Robert Szava-Kovats.** Assessment of stream sediment contamination by median sum of weighted residuals regression. Tartu, 2001.
17. **Heno Sarv.** Indigenous Europeans east of Moscow. Population and Migration Patterns of the Largest Finno-Ugrian Peoples in Russia from the 18th to the 20th Centuries. Tartu, 2002.
18. **Mart Külvik.** Ecological networks in Estonia — concepts and applications. Tartu, 2002.
19. **Arvo Järvet.** Influence of hydrological factors and human impact on the ecological state of shallow Lake Võrtsjärv in Estonia. Tartu, 2004.
20. **Katrin Pajuste.** Deposition and transformation of air pollutants in coniferous forests. Tartu, 2004.

21. **Helen Sooväli.** *Saaremaa waltz*. Landscape imagery of Saaremaa Island in the 20th century. Tartu, 2004.
22. **Antti Roose.** Optimisation of environmental monitoring network by integrated modelling strategy with geographic information system — an Estonian case. Tartu, 2005.
23. **Anto Aasa.** Changes in phenological time series in Estonia and Central and Eastern Europe 1951–1998. Relationships with air temperature and atmospheric circulation. Tartu, 2005.
24. **Anneli Palo.** Relationships between landscape factors and vegetation site types: case study from Saare county, Estonia. Tartu, 2005.
25. **Mait Sepp.** Influence of atmospheric circulation on environmental variables in Estonia. Tartu, 2005.
26. **Helen Alumäe.** Landscape preferences of local people: considerations for landscape planning in rural areas of Estonia. Tartu, 2006.
27. **Aarne Luud.** Evaluation of moose habitats and forest reclamation in Estonian oil shale mining areas. Tartu, 2006.
28. **Taavi Pae.** Formation of cultural traits in Estonia resulting from historical administrative division. Tartu, 2006.
29. **Anneli Kährik.** Socio-spatial residential segregation in post-socialist cities: the case of Tallinn, Estonia. Tartu, 2006.
30. **Dago Antov.** Road user perception towards road safety in Estonia. Tartu, 2006.
31. **Üllas Ehrlich.** Ecological economics as a tool for resource based nature conservation management in Estonia. Tartu, 2007.
32. **Evelyn Uuemaa.** Indicatory value of landscape metrics for river water quality and landscape pattern. Tartu, 2007.
33. **Raivo Aunap.** The applicability of gis data in detecting and representing changes in landscape: three case studies in Estonia. Tartu, 2007.
34. **Kai Treier.** Trends of air pollutants in precipitation at Estonian monitoring stations. Tartu, 2008.
35. **Kadri Leetmaa.** Residential suburbanisation in the Tallinn metropolitan area. Tartu, 2008.
36. **Mare Remm.** Geographic aspects of enterobiasis in Estonia. Tartu, 2009.
37. **Alar Teemusk.** Temperature and water regime, and runoff water quality of planted roofs. Tartu, 2009.
38. **Kai Kimmel.** Ecosystem services of Estonian wetlands. Tartu, 2009.
39. **Merje Lesta.** Evaluation of regulation functions of rural landscapes for the optimal siting of treatment wetlands and mitigation of greenhouse gas emissions. Tartu, 2009.
40. **Siiri Silm.** The seasonality of social phenomena in Estonia: the location of the population, alcohol consumption and births. Tartu, 2009.
41. **Ene Indermitte.** Exposure to fluorides in drinking water and dental fluorosis risk among the population of Estonia. Tartu, 2010.
42. **Kaido Soosaar.** Greenhouse gas fluxes in rural landscapes of Estonia. Tartu, 2010.

43. **Jaan Pärn.** Landscape factors in material transport from rural catchments in Estonia. Tartu, 2010.
44. **Triin Saue.** Simulated potato crop yield as an indicator of climate variability in Estonia. Tartu, 2011.
45. **Katrin Rosenvald.** Factors affecting EcM roots and rhizosphere in silver birch stands. Tartu, 2011.
46. **Ülle Marksoo.** Long-term unemployment and its regional disparities in Estonia. Tartu, 2011, 163 p.
47. **Hando Hain.** The role of voluntary certification in promoting sustainable natural resource use in transitional economies. Tartu, 2012, 180 p.
48. **Jüri-Ott Salm.** Emission of greenhouse gases CO_2, CH_4, and N_2O from Estonian transitional fens and ombrotrophic bogs: the impact of different land-use practices. Tartu, 2012, 125 p.
49. **Valentina Sagris.** Land Parcel Identification System conceptual model: development of geoinfo community conceptual model. Tartu, 2013, 161 p.
50. **Kristina Sohar.** Oak dendrochronology and climatic signal in Finland and the Baltic States. Tartu, 2013, 129 p.
51. **Riho Marja.** The relationships between farmland birds, land use and landscape structure in Northern Europe. Tartu, 2013, 134 p.
52. **Olle Järv.** Mobile phone based data in human travel behaviour studies: New insights from a longitudinal perspective. Tartu, 2013, 168 p.
53. **Sven-Erik Enno.** Thunderstorm and lightning climatology in the Baltic countries and in northern Europe. Tartu, 2014, 142 p.
54. **Kaupo Mändla.** Southern cyclones in northern Europe and their influence on climate variability. Tartu, 2014, 142 p.
55. **Riina Vaht.** The impact of oil shale mine water on hydrological pathways and regime in northeast Estonia. Tartu, 2014, 111 p.
56. **Jaanus Veemaa.** Reconsidering geography and power: policy ensembles, spatial knowledge, and the quest for consistent imagination. Tartu, 2014, 163 p.
57. **Kristi Anniste.** East-West migration in Europe: The case of Estonia after regaining independence. Tartu, 2014, 151 p.
58. **Piret Pungas-Kohv.** Between maintaining and sustaining heritage in landscape: The examples of Estonian mires and village swings. Tartu, 2015, 210 p.
59. **Mart Reimann.** Formation and assessment of landscape recreational values. Tartu, 2015, 127 p.
60. **Järvi Järveoja.** Fluxes of the greenhouse gases CO_2, CH_4 and N_2O from abandoned peat extraction areas: Impact of bioenergy crop cultivation and peatland restoration. Tartu, 2015, 171 p.
61. **Raili Torga.** The effects of elevated humidity, extreme weather conditions and clear-cut on greenhouse gas emissions in fast growing deciduous forests. Tartu, 2016, 128 p.
62. **Mari Nuga.** Soviet-era summerhouses On homes and planning in post-socialist suburbia. Tartu, 2016, 179 p.

63. **Age Poom.** Spatial aspects of the environmental load of consumption and mobility. Tartu, 2017, 141 p.
64. **Merle Muru.** GIS-based palaeogeographical reconstructions of the Baltic Sea shores in Estonia and adjoining areas during the Stone Age. Tartu, 2017, 132 p.
65. **Ülle Napa.** Heavy metals in Estonian coniferous forests. Tartu, 2017, 129 p.
66. **Liisi Jakobson.** Mutual effects of wind speed, air temperature and sea ice concentration in the Arctic and their teleconnections with climate variability in the eastern Baltic Sea region. Tartu, 2018, 118 p.
67. **Tanel Tamm.** Use of local statistics in remote sensing of grasslands and forests. Tartu, 2018, 106 p.
68. **Enel Pungas.** Differences in Migration Intentions by Ethnicity and Education: The Case of Estonia. Tartu, 2018, 142 p.
69. **Kadi Mägi.** Ethnic residential segregation and integration of the Russian-speaking population in Estonia. Tartu, 2018, 173 p.
70. **Kiira Mõisja.** Thematic accuracy and completeness of topographic maps. Tartu, 2018, 112 p.
71. **Kristiina Kukk.** Understanding the vicious circle of segregation: The role of leisure time activities. Tartu, 2019, 143 p.
72. **Kaie Kriiska.** Variation in annual carbon fluxes affecting the soil organic carbon pool and the dynamics of decomposition in hemiboreal coniferous forests. Tartu, 2019, 146 p.
73. **Pille Metspalu.** The changing role of the planner. Implications of creative pragmatism in Estonian spatial planning. Tartu, 2019, 128 p.
74. **Janika Raun.** Mobile positioning data for tourism destination studies and statistics. Tartu, 2020, 153 p.
75. **Birgit Viru.** Snow cover dynamics and its impact on greenhouse gas fluxes in drained peatlands in Estonia. Tartu, 2020, 123 p.